Chapter 1

THE SUN

R.C. Altrock
H.L. DeMastus
J.W. Evans
S.L. Keil, Capt., USAF
D.F. Neidig
R.R. Radick
G.W. Simon

Radiant energy from the sun determines the surface temperature of the earth and supplies virtually all the energy for natural processes on the earth's surface and in its atmosphere. The sun is about 5×10^9 years old and geological and paleontological evidence indicates it has shone with its present intensity for about a billion years. The solar radiation is, however, not absolutely constant. There are short-period fluctuations in ultraviolet and x-ray radiation and in corpuscular emission that induce complex responses in the earth's atmosphere. In this chapter, solar characteristics and activity are identified; other chapters deal with the geophysical responses themselves. We shall discuss first the *quiet sun*, then solar activity.

1.1 THE SUN'S "STEADY-STATE" BEHAVIOR (THE QUIET SUN)

Although all observable solar features change on timescales of seconds to days, the statistical description of many such features taken together remains unchanged over substantial periods of time. These "steady-state" features of the so-called quiet sun are described here.

1.1.1 Basic Characteristics

The sun is a relatively small, faint, cool star at an average distance of 1.49×10^8 km from the earth. Its mass is 1.99×10^{33} g. Composition of the outer layers by mass is approximately 73% H, 25% He, and 2% other elements [Allen, 1973]. Table 1-1 gives the run of temperature, density, mass concentration, energy generation, and pressure as functions of radius [Allen, 1973]. The total solar luminosity is 3.83×10^{33} erg/s.

A schematic cross-section through the sun is shown in Figure 1-1. Energy is generated in the solar core by nuclear reactions. The primary reaction is the fusion of hydrogen nuclei to form helium nuclei ($4H^1 \rightarrow He^4$). For every gram of hydrogen entering the reaction, 0.007 g is converted into energy. To produce the solar luminosity, about 4.3×10^{12} g/s must be converted to energy.

The energy generated in the core is transferred outward by radiation. Because of the high densities, the radiation is absorbed and re-emitted many times on its outward journey. Radiation that began in the core as high energy gamma rays is degraded by these successive absorptions and re-emissions until they finally emerge as visible radiation characteristics of the solar surface. However, the energy is not carried all the way to the surface as radiation. As it moves outward from the core, the temperature, density, and pressure drop. As the temperature drops, free electrons can be trapped by atoms into bound states, causing an increase in the opacity. Thus radiation becomes less effective in transporting energy. A large temperature gradient results and

Table 1-1. Solar structure as function of radius [Allen, 1973].

	r	T	ρ	M_r	L_r	log P
R_o	10^3 km	10^6 K	g/cm^3	M_o	L_o	dyn/cm^2
0.00	0	15.5	160	0.000	0.00	17.53
0.04	28	15.0	141	0.008	0.08	17.46
0.1	70	13.0	89	0.07	0.42	17.20
0.2	139	9.5	41	0.35	0.94	16.72
0.3	209	6.7	13.3	0.64	0.998	16.08
0.4	278	4.8	3.6	0.85	1.00	15.37
0.5	348	3.4	1.00	0.94	1.000	14.67
0.6	418	2.2	0.35	0.982	1.000	14.01
0.7	487	1.2	0.08	0.994	1.000	13.08
0.8	557	0.7	0.018	0.999	1.000	12.18
0.9	627	0.31	0.0020	1.000	1.000	10.94
0.95	661	0.16	0.0^34	1.000	1.000	9.82
0.99	689	0.052	0.0^45	1.000	1.000	8.32
0.995	692.5	0.031	0.0^42	1.000	1.000	7.68
1.000	696.0	0.006	0.0	1.000	1.000	—

T = temperature; ρ = density; P = pressure; M_r = mass within radius 4; L_r = energy generation within radius r; M_o, R_o, L_o = mass, radius, energy generation of whole Sun, with $M_o = 1.99 \times 10^{33}$g and $L_o = 3.83 \times 10^{33}$ergs.

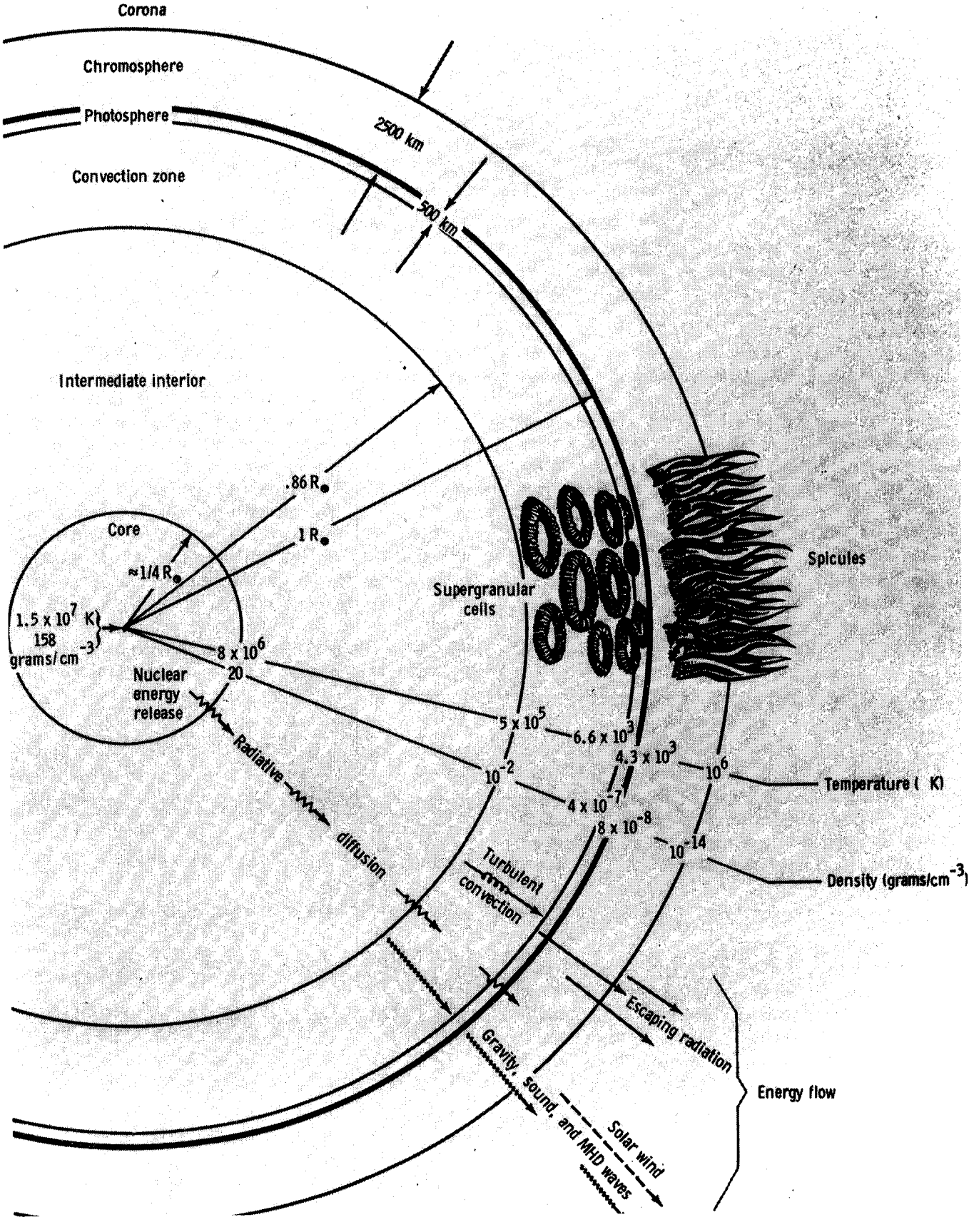

Figure 1-1. Idealized general solar properties, structure, and modes of outward energy flow. The features shown are not to scale and provide a qualitative picture only [Gibson, 1973].

convection becomes the primary energy transport mechanism. The exact depth at which this occurs is model dependent. However, observations clearly show that this *convection zone* reaches the solar surface and that at least 3 or 4 scales of convection are present. Near the solar surface, radiation can escape into space and it again becomes the primary energy transport mechanism.

Attempts to make accurate measurements of the solar diameter have led to the discovery of global solar oscillations. The observed periods agree approximately with theoretically predicted radial p-mode oscillations. Table 1-2 compares some observed periods of global oscillations with predictions based upon a theoretical solar model [Christensen-Dalsgaard and Gough, 1976]. A summary of attempts to measure global solar oscillations can be found in Hill [1979]. These modes of oscillation can be used in a manner

Table 1-2. Observed and theoretical modes of solar oscillations [Christensen-Dalsgaard and Gough, 1976].

Periods of Solar Oscillations (min)								
		l = 0		l = 2		l = 4		l = 2	
1973	1975	Mode	Period	Mode	Period	Mode	Period	Mode	Period
		p_1	62.7						
			(63.9)					g_1	55.1
52	47.9			f	46.0				
				p_1	42.2	f	39.6		
		p_2	43.8		(42.3)	p_1	38.0	g_2	61.5
33		p_3	32.6						
			(31.8)	p_2	34.3			g_3	70.9
	30.3					p_2	29.3		
		p_4	26.0	p_3	26.7			g_4	81.8
23.8						p_3	23.4		
	21.0	p_5	21.0						
			[21.5]	p_4	21.5			g_5	93.0
						p_4	19.5		
		p_6	18.2	p_5	17.9			g_6	105
16.7	17.1					p_5	16.3		
		p_7	15.8	p_6	16.0			g_7	117
	14.6		[15.4]			p_6	14.6		
		p_8	14.0	p_7	14.1			g_8	130
13.3						p_7	13.0		
		p_9	12.5	p_8	12.6			g_9	142
11.9	11.8					p_8	11.7		
		p_{10}	11.3	p_9	11.4			g_{10}	154
									(147)
10.4	10.5	p_{11}	10.4	p_{10}	10.4			g_{11}	167
									(159)
		p_{12}	9.55					g_{12}	180
									(171)
9.2	8.8	p_{13}	8.84						
			[9.12]						
		p_{14}	8.52						
	7.9	p_{15}	7.99						
7.6		p_{16}	7.53						
7.0	7.2	p_{17}	7.12						
		p_{18}	6.75						
		p_{19}	6.41						
		p_{20}	6.10						

The periods headed 1973 and 1975 are from observations by Hill, Stebbins, and Brown [1975] and are accurate to ~ 5%. Those periods not reported in the publication were kindly supplied by Profesor Hill. Periods in the other columns were obtained theoretically using a solar model with Z = 0.02, except those in parenthesis which are periods of oscillation of a model with Z = 0.04. The periods in square brackets were obtained by repeating the computation with Z = 0.02 using a different distribution of mesh points. (Reprinted with permission from Macmillan Journals Ltd. © 1976.)

analogous to terrestrial seismology to probe the deep interior of the sun. This should eventually permit us to refine the model shown in Table 1-1 and place better constraints on theoretical models of the solar interior.

The total solar irradiance is quantitatively defined as the amount of radiant energy at all wavelengths received per unit time and area at the top of the earth's atmosphere, corrected to the mean earth-sun distance, and is customarily expressed in units of watts per square meter (W/m^2). The term *solar constant* is also used occasionally to denote this

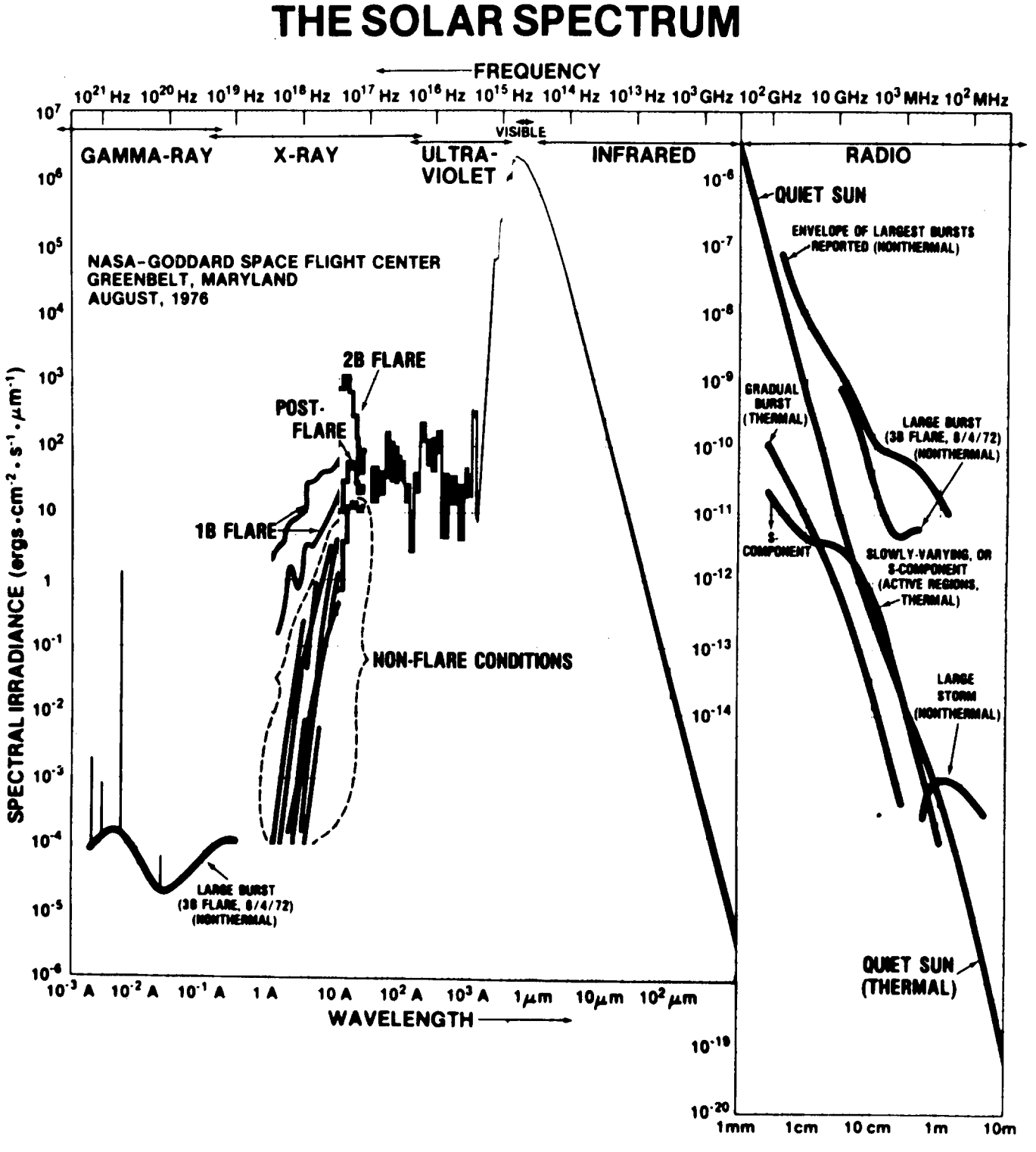

Figure 1-2. Spectral distribution of solar irradiance [White, 1977].

radiant flux but is somewhat misleading, since the total solar irradiance seems to fluctuate slightly. The best measurement to date of the total solar irradiance, 1368 ± 7 W/m^2, was obtained in 1980 using radiometers aboard the NASA Solar Maximum Mission (SMM) satellite.

More than 70% of the solar irradiance is concentrated in the near ultraviolet, visible, and near infrared portions of the spectrum lying between the atmospheric transmission cut-offs near 0.32 μm and 1.0 μm. Since most of this radiation reaches the earth's surface, a large fraction of its energy enters the lower atmosphere through the evaporation-precipitation cycle of water. About 2% of the solar irradiance appears at ultraviolet and x-ray wavelengths shorter than 0.32 μm. This radiation is all strongly absorbed in the upper atmosphere where it drives several important photochemical reactions, including ozone production. The remainder of the solar irradiance appears at infrared and radio wavelengths longer than 1.0 μm. Much of this radiation, especially in the infrared, is strongly absorbed by atmospheric water vapor and carbon dioxide and thus contributes to the energy budget of the lower atmosphere.

Figure 1-2 illustrates the spectral distribution of the solar irradiance. A complete description of the ultraviolet and radio portions of the solar irradiance will be found in Chapters 2 and 11.

1.1.2 Solar Rotation

The rotation period of the sun is a function of solar latitude, varying from about 24 days at the equator to 34 days at the pole. This variation is called *differential rotation*. Taking into account the earth's orbital motion, an effective period of 27 days is usually satisfactory for predicting rotation recurrences of solar-terrestrial disturbances. Because the sun's axis of rotation is inclined only 7° to the plane of the earth's orbit, most of the solar surface can be scanned in the course of one rotation.

When solar rotation is measured by following tracers (features on the solar surface such as sunspots) one observes faster rotation rates than from the Doppler shifts of solar spectral lines. Figure 1-3 shows the latitudinal dependence of rotation rate measured by tracers compared to the Doppler shift of lines [Wilcox and Howard, 1970]. Furthermore, Doppler measurements show that the differential rotation varies with time, and seems to have large eddies or cells imbedded in it. These temporal variations can be as large as the variation in latitude. Evidence has also been found for toroidal oscillations superposed on the solar rotation [Howard and LaBonte, 1980].

Differential rotation probably has its origin in the interaction between convection and rotation. This same interaction underlies most of the magnetic activity observed on the sun (Section 1.2.2).

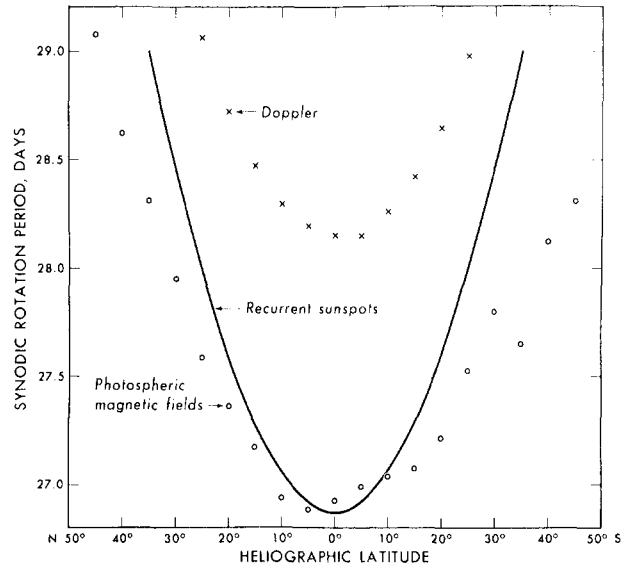

Figure 1-3. Solar differential rotation for sunspots (solid curve), large scale photospheric magnetic fields (circles) and quiet photosphere (crosses) [Wilcox and Howard, 1970].

1.1.3 The Solar Atmosphere

Because the sun is gaseous throughout, there is no rigid boundary marking the start of the atmosphere and end of the interior. However, a definite optical boundary, below which we cannot see, exists and is commonly referred to as the solar surface. As can be seen from Table 1-1, the solar temperature decreases outward from the core until we reach this optical surface. For a few hundred kilometers above this level the temperature continues to decrease. However, at about 400 km one reaches the *temperature minimum*, above which the temperature again begins to increase with increasing height. Although no rigid boundaries exist, it is convenient to divide the solar atmosphere into layers having characteristic temperatures and densities. Moving outward from the optical surface these layers are known as the *photosphere, chromosphere, transition zone,* and *corona*. Each of these regions is discussed below.

1.1.3.1 The Photosphere. The photosphere is the apparent solar surface, with a very sharply defined limb, seen by ordinary observations in white light. Its location with respect to other solar features is shown in Figure 1-1. Its diameter, usually considered to be the diameter of the sun, is 1.391 × 10^6 km. Practically all of the solar mass is contained within the radius of the photosphere. Figure 1-4 shows the variation of temperature, density, and pressure in a standard model of the lower solar atmosphere. Height is given in kilometers above a depth in the atmosphere for which the probability of a photon escaping is 1/e. The thickness of the photosphere is only about 100 km, or 0.014% of R_o, where R_o is the solar radius. Below the photosphere

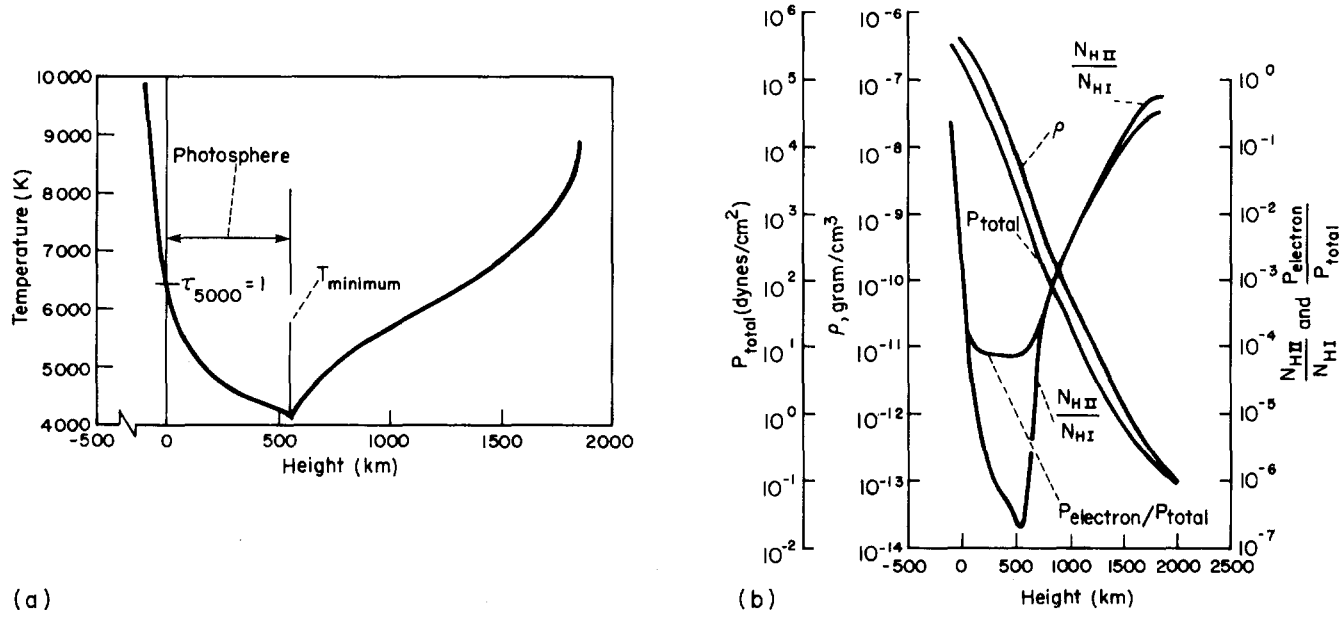

Figure 1-4. Gas properties versus height (HSRA model)[Gingerich, 1971]. (a) Temperature as a function of height. (b) Pressure, density, electron pressure, and hydrogen ionization as functions of height.

the solar gas is opaque. This opacity is primarily due to a small concentration of negative hydrogen ions in the region immediately below the photosphere. These negative ions act as continuous absorbers over a great range of wavelengths, absorbing most of the intense radiation from deeper layers in the sun. The resulting accumulation of thermal energy in this layer sets up a system of convective currents that transports the excess energy through the negative hydrogen barrier. The energy is then reradiated into the relatively transparent gases above the photosphere and, hence, into space. Penetration of these convective elements (*granules*) into the photosphere gives rise to the granular appearance of the solar surface shown in Figure 1-5. Similar opacity barriers which exist deeper in the sun cause other larger scales of convective motions. The most obvious of these is the *supergranulation* shown in Figure 1-6. Figure 1-7 is a schematic diagram of the various scales of motion present in the solar atmosphere.

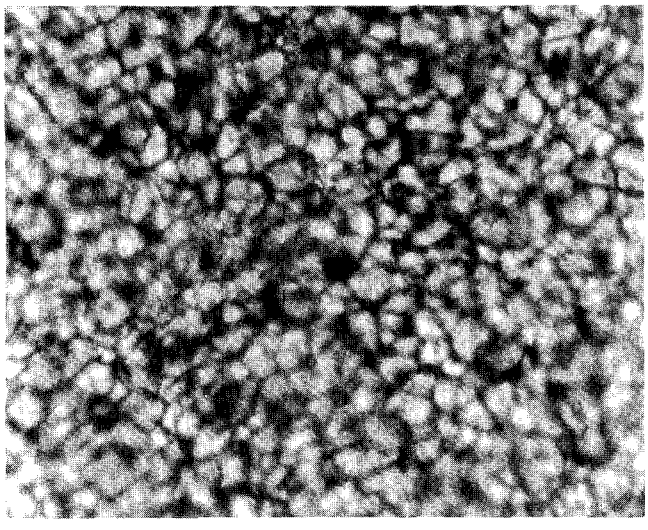

Figure 1-5. Photospheric granulation and sunspot structure photographed with 180 ft. focal length tower telescope at the National Solar Observatory at Sacramento Peak.

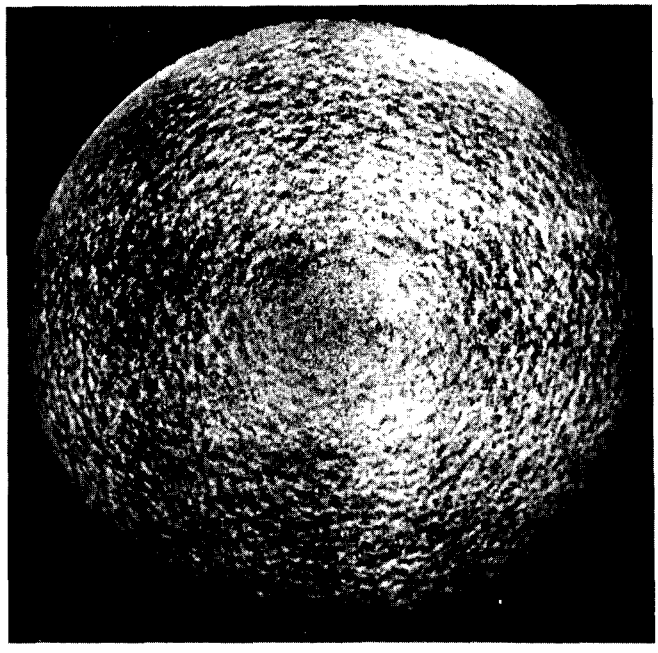

Figure 1-6. Velocity spectroheliogram obtained in Ca 6103 Å, showing supergranulation structure on solar surface. Supergranules have diameters of about 30 Mm and lifetimes of 1-2 days.

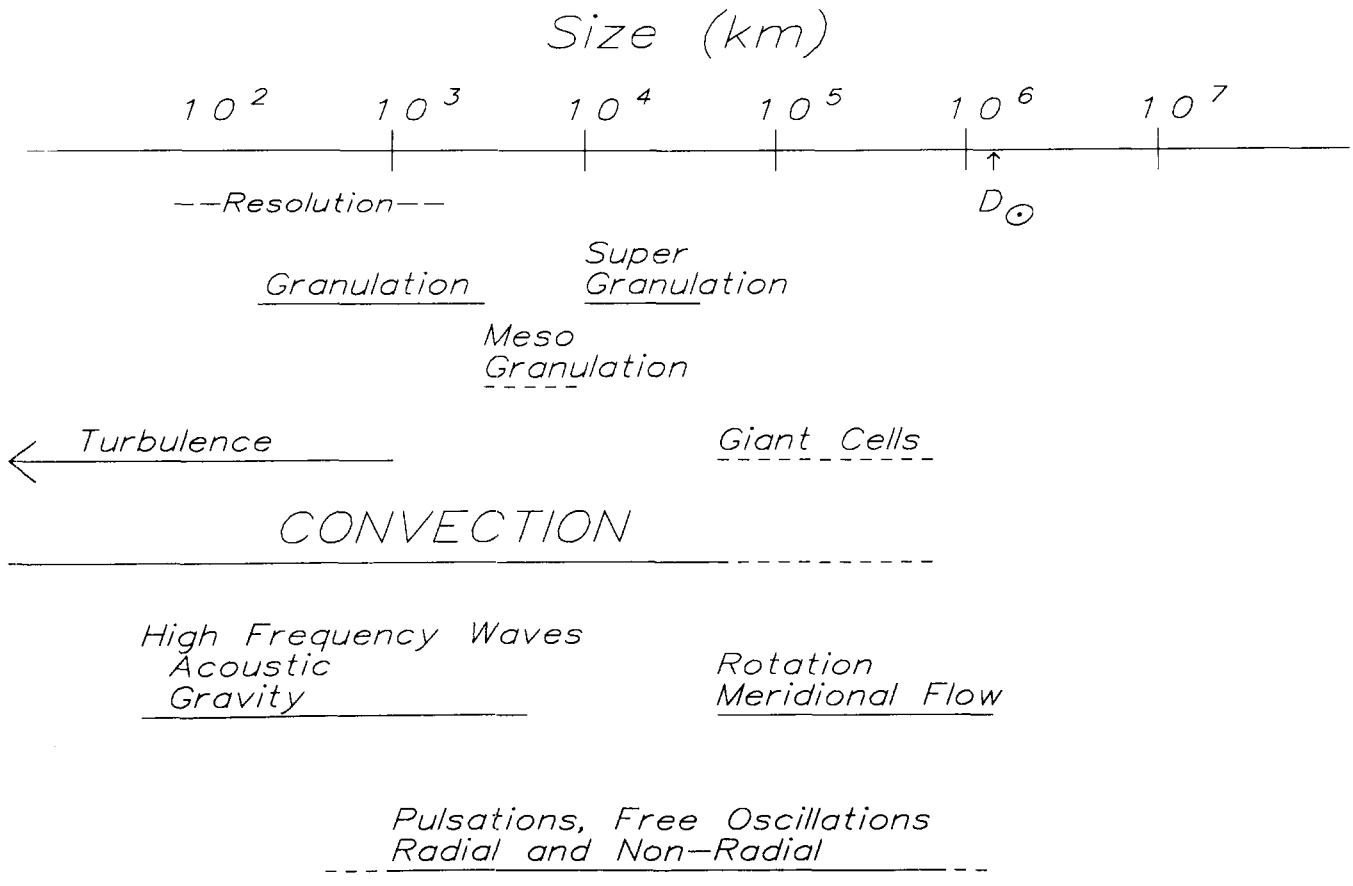

Figure 1-7. This schematic diagram shows the horizontal size of various motions present in the solar atmosphere. Also shown is an approximate range for the resolution limit of ground-based observations. The smaller sizes indicated for resolution are only achieved using special techniques such as speckle interferometry or active optical systems. Typical resolution for conventional telescopes is limited by turbulence in the terrestrial atmosphere to approximate one arcsecond or about 720 km on the sun. The scales shown with the solid lines indicate an approximate range, while the dashed lines indicate sizes either predicted theoretically or that have been only tentatively observed.

Because the opaque gas composing the photosphere absorbs and reradiates approximately as a black body, the photosphere emits an essentially continuous spectrum, or *continuum*. Sharply tuned absorptions by the various atoms in and above the photosphere give rise to thousands of dark lines (Fraunhofer lines) superposed on the continuum. This line absorption spectrum, shown in Figure 1-8, is the source of most information on the abundance of the various elements and the physical state of the solar atmosphere. Although the lines of a number of atoms are unobservable through the terrestrial atmosphere, all the natural chemical elements known on earth probably exist in the sun. Their relative abundances, however, differ radically.

The principal region of line absorption is a layer about 400 km thick just above the visible surface of the photosphere. Spectra with high spatial resolution on the sun as shown in Figure 1-9 show small-scale wiggles due to Doppler shifts induced by mass motions in the line formation region. Analysis of these *wiggly lines* has revealed several physical processes occurring on the sun.

The granules of Figure 1-5 are evidence of convective overshooting into the stable photosphere from deeper layers.

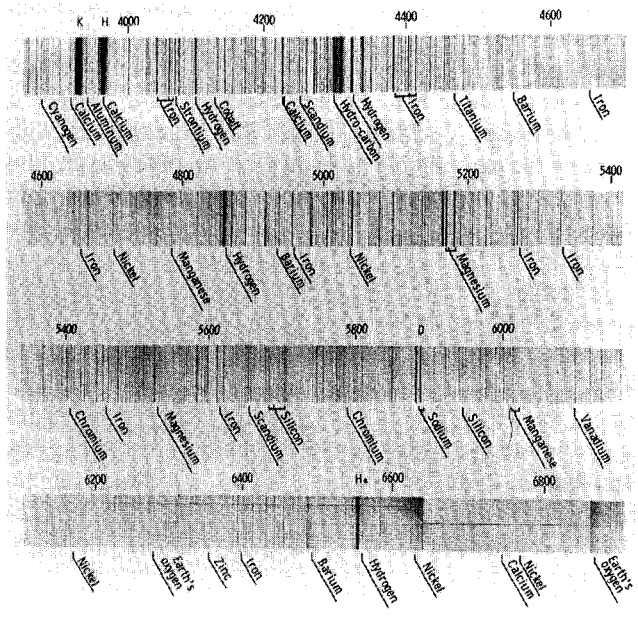

Figure 1-8. The Fraunhofer line absorption spectrum of the solar atmosphere.

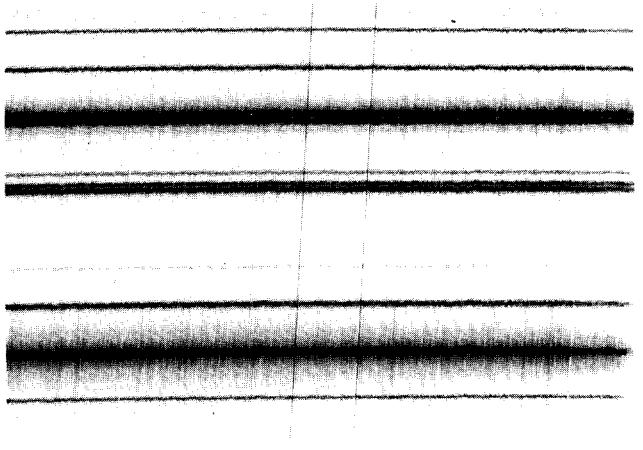

Figure 1-9. The spectral region around the Mg B lines at 5167 Å and 5172 Å is shown. The verticle axis is wavelength and the horizontal axis is distance along the slit. The dark horizontal bars are absorption lines.

An average granule has a diameter of about 1.4 arcsec or 1 Mm. Granules typically live for 8 minutes and reach velocities near 2 km/s. Most granules lose their temperature excess after rising only 50 to 100 km into the photosphere, but their momentum carries them 100 or 200 km higher.

The supergranules shown in Figure 1-6 penetrate higher into the atmosphere but have much smaller vertical motions than granules. They are primarily observed as horizontal flows in the chromospheric layers above the photosphere. Supergranules have diameters of approximately 30 Mm and lifetimes of 1-2 days. Evidence has recently been found for two other scales of convection: mesogranulation [November et al., 1981] with a scale of 5-10 Mm, and giant cells perhaps 100 Mm in diameter.

In addition to revealing various modes of convection, wiggly line spectra show that the sun oscillates in a number of different modes. Oscillatory modes with large coherent wave systems having periods near 300 s are observed in the photosphere and overlying chromosphere. Such data are compared with a theoretical non-radial acoustic spectrum in Figure 1-10. These modes have most of their energy concentrated in the underlying convection zone, and deviations of predicted modes from observed modes can lead to better models of the convection zone. The 300 s oscillations are evanescent in the photosphere (below the temperature minimum shown in Figure 1-4). At the higher temperatures found in the chromosphere, the waves become propagating and higher frequency acoustic waves are observed. The mechanical energy in these waves may be responsible for the temperature increase in the chromosphere and higher layers.

1.1.3.2 The Chromosphere. The chromosphere is a layer, several thousand kilometers thick, of transparent glowing gas above the photosphere. Many of the phenomena occurring in the photosphere also are manifest in the chromosphere. Because the density in the chromosphere continues to decrease with height (Figure 1-4) and is much lower than in the photosphere, magnetic fields and waves can have greater influence on the structure. Thus the chromosphere is even more inhomogeneous than the photosphere. Its continuous spectrum is extremely faint, and like

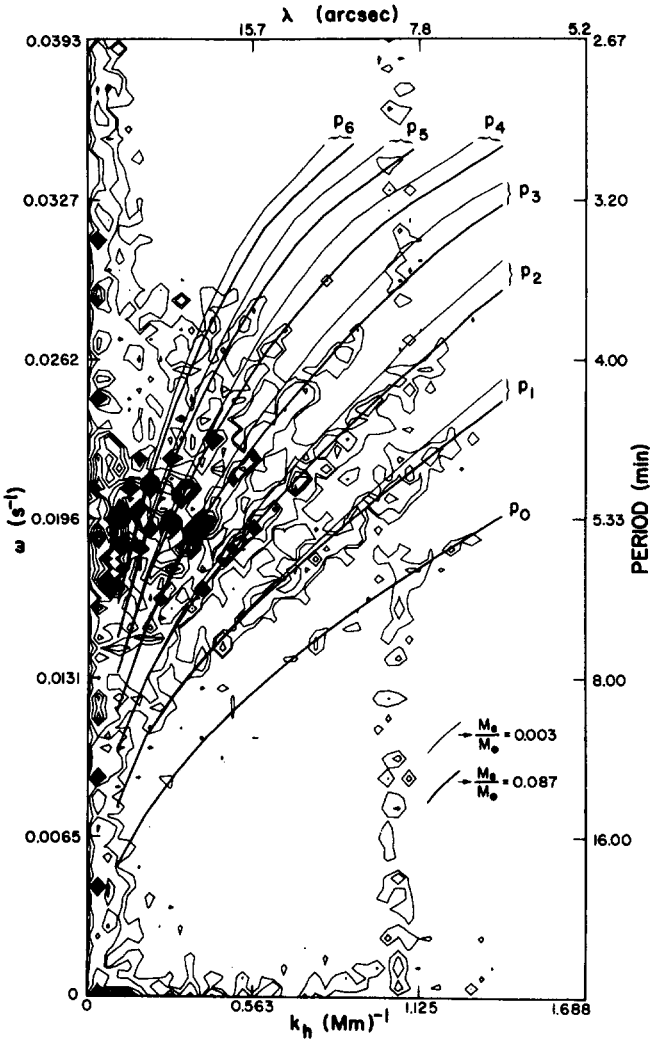

Figure 1-10. Comparison of an observed k-ω diagram with theoretical Eigenfrequencies for two model solar envelopes [Rhodes et al., 1977]. Contour intervals are 0.125, 0.25, 0.75, 1.75, etc. m^2s^{-2}. Observations were made on the magnetically insensitive line Fe I λ 5576.10 using the vacuum tower telescope at the National Solar Observatory at Sacramento Peak. (Reprinted with permission from the American Astronomical Society © 1977.)

all solar features above the photosphere, it can be observed normally only by isolating the light of one of its strong lines, usually the red Hα line at 6563 Å (Fraunhofer C line) or the line of CA II at 3934 Å (Fraunhofer K).

The rise in chromospheric temperature with height can be understood in terms of a nonradiative energy input into the atmosphere via mechanical energy generated in the convection zone. Acoustical waves propagate outward and can form shocks in the low density chromosphere, creating more energetic collisions between particles. The low density also leads to a relative enhancement in the ability of magnetic fields to carry energy in the form of waves. These mechanisms combine to heat the chromosphere from approximately 4300 K at its base to over 20 000 K in about 2 Mm.

Similar to the granulation patterns observed in the photosphere, a *chromospheric network* can be observed in chromospheric lines. Figure 1-11 shows the appearance of this network in Hα and Ca II. The scale of this network corresponds fairly closely to that of supergranulation, and the bright regions of the chromospheric network correlate well with supergranular boundaries. At sub-photospheric densities the supergranules are capable of pushing magnetic flux tubes to their boundaries while in the chromosphere the fields dominate the gas. If heating occurs preferentially near the field lines, the appearance of the network can be explained. The network is also the location of *spicules* which are brilliant flames of gas that project upward for approximately 10 Mm and live for 2 to 5 minutes. Figure 1-12 shows how these spicules appear at the limb of the sun. Spicules may provide the primary path for moving energy and material into the corona.

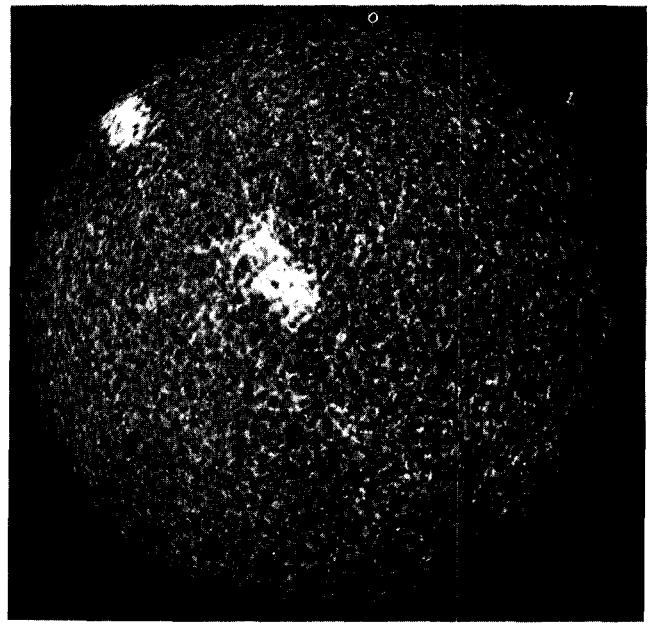

Figure 1-11. Ca II spectroheliograms made on the violet side of Ca II line at 3934 Å. The network of bright emission is clearly evident, and outlines the boundaries of supergranules seen in Figure 1-6.

1.1.3.3 The Transition Region. At the top of the chromosphere, approximately 1.7 Mm above the temperature minimum, the temperature begins a sudden steep rise to coronal values. In the next few megameters it rises from 25 000 K to near 2×10^6 K. This steep temperature rise is called the transition region. Because this transition occurs in such a narrow zone of the solar atmosphere, it is very difficult to measure the physical height boundaries accurately. It is also very hard to observe this region, since its spectral lines are in the EUV and can be studied only from satellite and rocket observations. Thus the amount of data available to date is very limited. We show in Figure 1-13 a profile of temperature vs height from the photosphere to the low corona with some transition zone spectral lines indicated. The slope of the rise and the location of its onset are functions of solar activity, being steeper and lower in the atmosphere in active regions (Section 1.2.3.1) than on the quiet sun. EUV photographs of the transition zone obtained by Skylab are shown in Figure 1-14. For further information on this region, including models, see Jordan [1981], Zirker [1977], Athay [1976], and Bonnet [1981].

1.1.3.4 The Corona. *Physical Properties*: Above the transition region and extending out into interplanetary space is the faintly visible solar corona. Long seen only during the few seconds or minutes of total solar eclipses, the true nature of this outer atmosphere has only in recent years been recognized. Dominated by temperatures of one to two million degrees, magnetically-induced motions, sudden releases of energy, and explosive expansion into the surrounding vacuum of space, this entity has strong implications for the energy balance of near-solar space and planetary environments.

The corona is heated from below by mechanical, electrical or magnetic dissipation. The exact nature of the heating has not yet been discovered. Favorite candidates are shock waves produced by the upward surging of granules

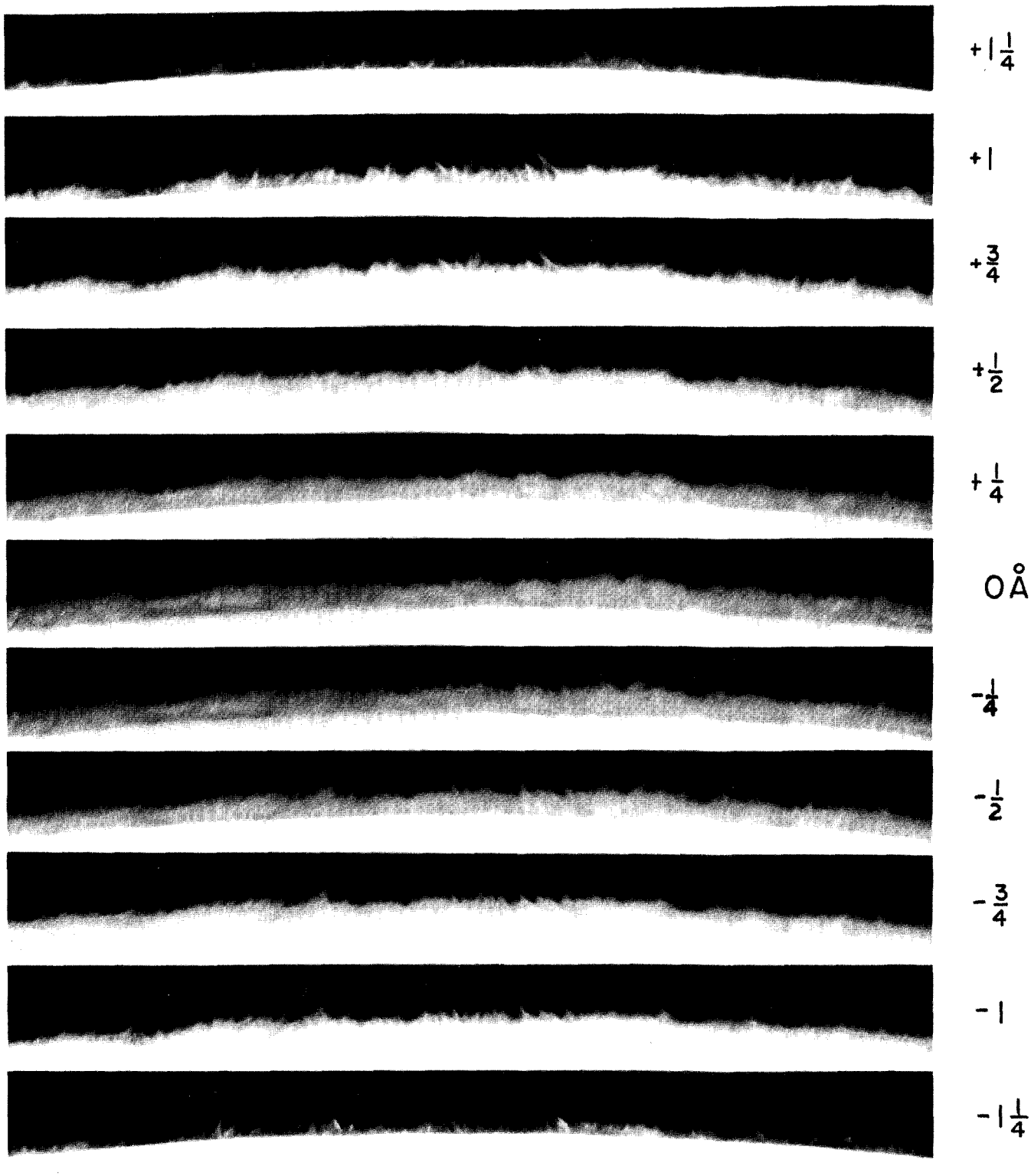

Figure 1-12. Spicules at the limb observed in Hα. These narrow tongue-like flames extend 5-19 Mm above the limb and live for 2–5 minutes.

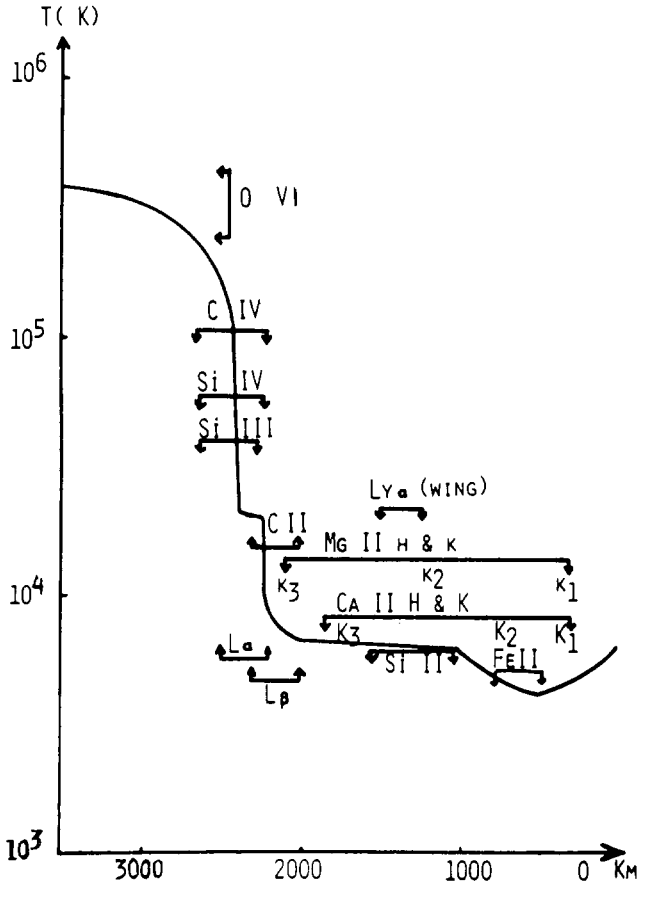

Figure 1-13. An average quiet sun temperature distribution from photosphere (0 km), through the temperature minimum (400 km), chromosphere (500-2000 km), and transition zone (2000-2500 km), and into the low corona (3000 km up), derived from Vernazza et al. [1981].

into the photosphere or by propagating waves or oscillations induced by them or by spicules. Other recent speculation has centered on the dissipation of Alfvén waves being propagated upward from the turbulent photosphere along magnetic lines of force. The end result of this heating, whatever its source, is an increase in temperature to near 2×10^6 K in the low corona. The temperature decreases slowly above that level. This extreme heat causes the outer parts of the corona to "boil away" into the near-vacuum of interplanetary space. Coronal heating is reviewed in Jordan [1981].

Observations of the corona (Figure 1-15) indicate that it is highly inhomogeneous. Different regions, such as *streamers* (radially-elongated bright areas—Section 1.2) and *coronal holes* (dark areas—Section 1.2), show small variations in temperature (on the order of 30%) from area to area, but large variations in density, up to one to two orders of magnitude. These variations become more pronounced with height.

Models of the corona are controversial and complex. Early one-dimensional models have now given way to two- and three-dimensional models representing streamers, coronal holes, magnetic loops, prominence cavities, and time-dependent variations in coronal transients.

Table 1-3 presents a simple model of a coronal hole and the quiet corona. Further information should be sought in Zirker [1977], White [1977], Allen [1973], Eddy [1978], and Jordan [1981].

Table 1-3. Model of corona in quiet sun and in coronal hole showing electron density vs height above the solar limb (R_o = 1.0) [Zirker, 1977].

	Quiet Sun ($T = 2.0 \times 10^6$ K)	Coronal Hole ($T = 1.5 \times 10^6$ K)
r/R_o	N_e (cm^{-3})	N_e (cm^{-3})
1.1	1.0×10^8	5.4×10^7
1.2	7.1×10^7	1.6×10^7
1.4	2.3×10^7	2.8×10^6
2.0	2.8×10^6	2.0×10^5
4.0	8.9×10^4	4.0×10^3
10.0	8.0×10^3	

Methods of Observation: Coronal observations are extremely difficult because of the requirement to eliminate the million-times-brighter light from the solar disk. Until the development of the coronagraph in the 1930s, the only observations of the faint coronal light (about as bright as the full moon) were made during total solar eclipses.

In the standard coronagraph, light spilling around an occulting disk is either passed through the narrow slit of a spectrograph to form a spectrum of the faint emission lines or through a narrow-band birefringent filter to form an image of the corona in an emission line, most often the green line of Fe XIV (5303 Å), and at times the red Fe X (6374 Å), or yellow Ca XV (5694 Å) lines. These lines have ionization temperatures of 1.5, 1.0, and 3.4×10^6 K, respectively. Figure 1-16 shows two filtergrams of the corona.

Photoelectric coronal observations from the ground are of two types. Observations of the emission-line corona made with a differential photometer at the National Solar Observatory at Sacramento Peak in New Mexico consist of circular scans around the limb at two or three heights. A sequence of such daily scans can be used to build up a picture of the low corona over a half solar rotation (Figure 1-17). Observations of the intermediate corona using light scattered by coronal electrons (also called the "K" corona) are made daily with the *K-coronameter* on Mauna Loa, Hawaii.

The corona can also be observed with radio telescopes (Chapter 11). Here the corona can be seen directly against the disk (there is no complicating "background light" as in the visible), and different heights can be probed by using different frequencies.

The discovery of coronal holes (Section 1.2.7.1), one of the major advances in solar physics in the past decade,

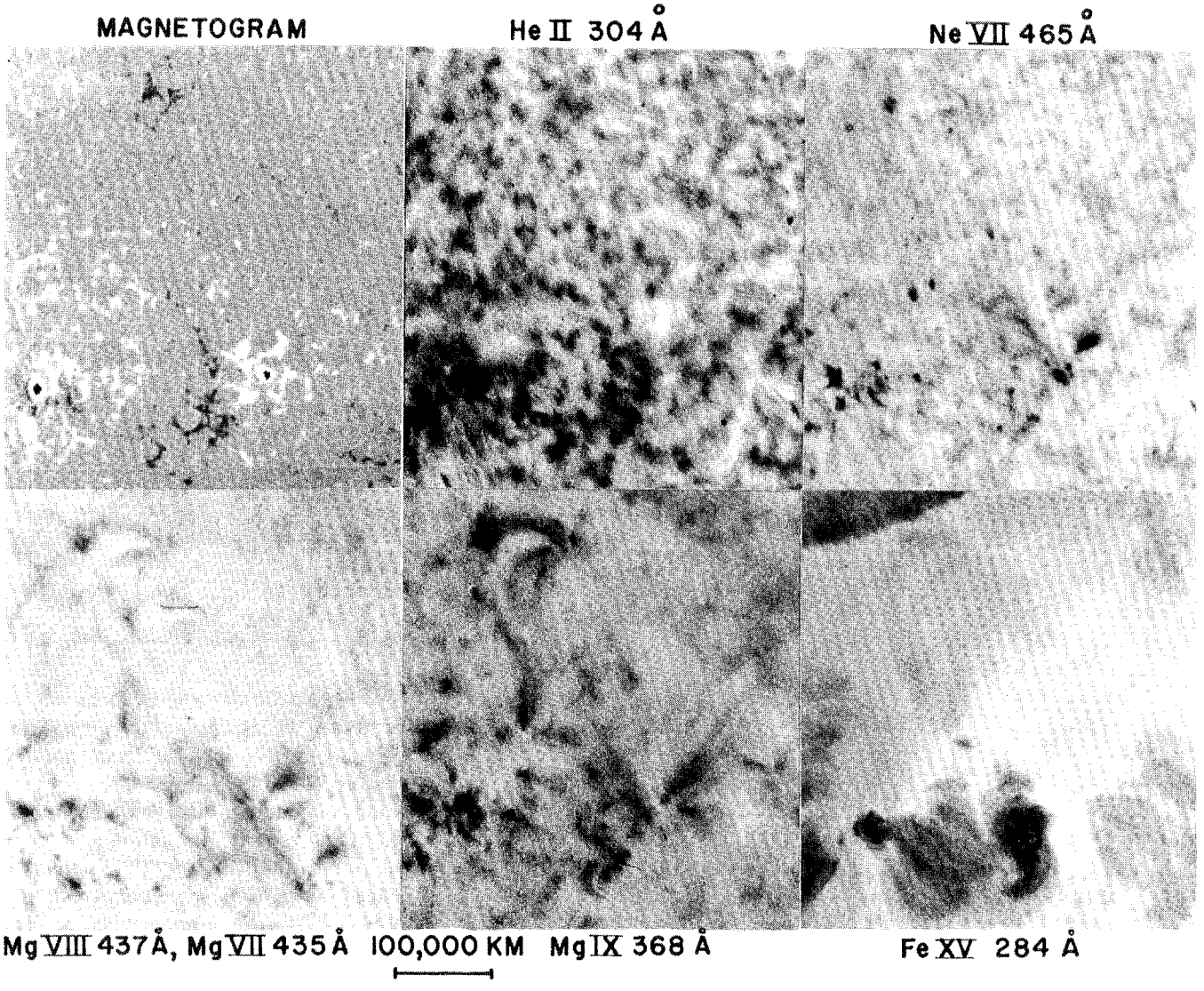

Figure 1-14. Spectroheliograms (EUV) made with a slitless spectrograph of lines in the transition zone obtained with Skylab, 1973–74. The Magnetogram is a ground-based observation.

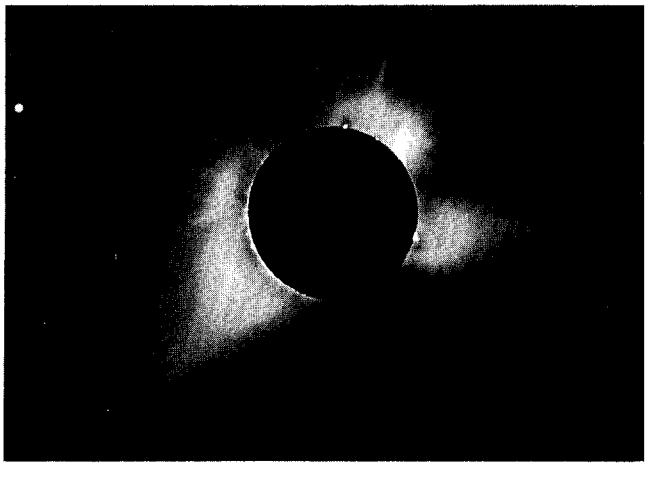

Figure 1-15. The Solar Corona. This photograph was taken at a solar eclipse with a filter that allows progressively more light to enter the camera as distance away from the solar limb increases. This greatly enhances the detail to be seen. Venus is visible on the left side (High Altitude Observatory).

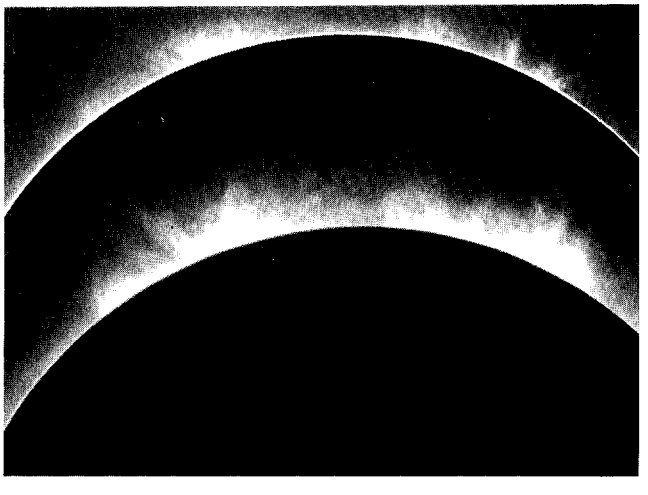

Figure 1-16. Two filtergrams of the solar limb as seen in the coronal lines Fe X, 6374 Å (above) and Fe XIV, 5303 Å (below) obtained with the new "one-shot" coronagraph at the National Solar Observatory at Sacramento Peak.

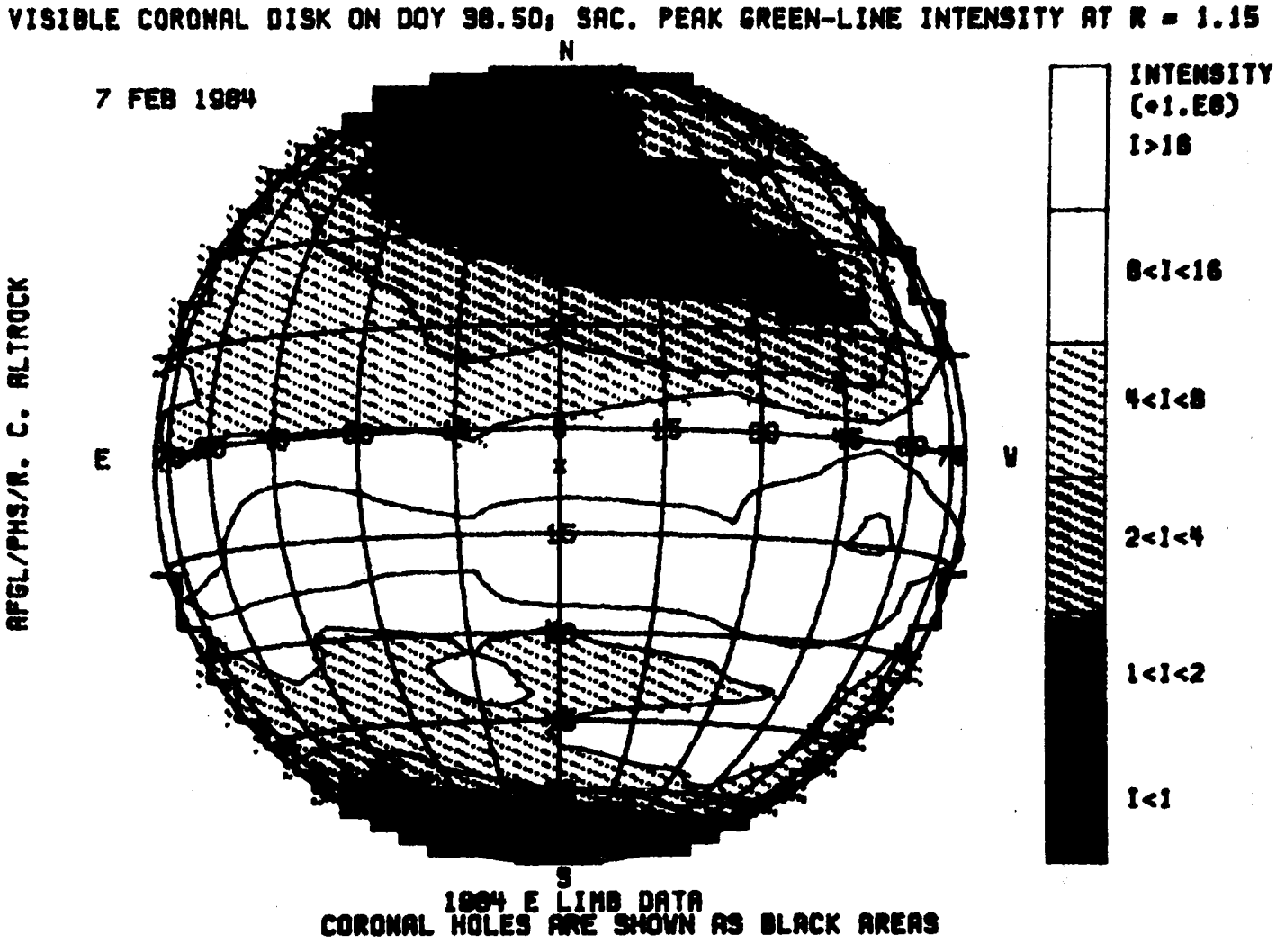

Figure 1-17. A "picture" of the green-line corona on 7 Feb 1984 obtained by allowing successive east-limb scans to rotate across the disk. Note the (black) polar coronal holes from which high speed solar wind streams flow. (National Solar Observatory at Sacramento Peak).

was made possible by satellite observations. The lack of a scattering and absorbing atmosphere at satellite altitudes made possible the first prolonged high-resolution solar observations in soft x rays. These Skylab observations and others revolutionized the understanding of coronal processes. Astronomers also use satellite images of the corona obtained in the extreme ultraviolet (EUV) with Skylab, and coronagraph observations in white light and emission lines both from Skylab and the Solar Maximum Mission satellite (SMM).

Indirect observations of the corona can be made on the disk in some spectral lines of helium, most notably that of 10830 Å. The population of certain atomic states of chromospheric helium is partially controlled by conditions in the overlying corona, and so coronal holes are marginally detectable in this line. A daily 10830 Å patrol (Figure 1-18) is operated at the National Solar Observatory facility on Kitt Peak, Arizona.

Another source of data concerning the corona and the near-solar interplanetary medium (IPM) is the scintillation of radio stars as observed through the corona/IPM. Semi-empirical relations between the signal fluctuation of a radio star and the turbulence generated at a given point in the IPM by solar wind flow (Chapter 3) have allowed investigators at the University of California, San Diego (UCSD), to produce low-resolution three-dimensional pictures of the solar wind flow within one astronomical unit (the distance from the earth to the sun) of the earth.

1.2 THE ACTIVE SUN

Although the quiet sun is of immense astronomical interest because it is the only star whose spatial features are readily resolvable with earth-bound telescopes, most of the sun's geophysical effects (except for the basic solar irradiance) result from solar activity. In this section we shall discuss phenomena related to the sun's magnetic field, for

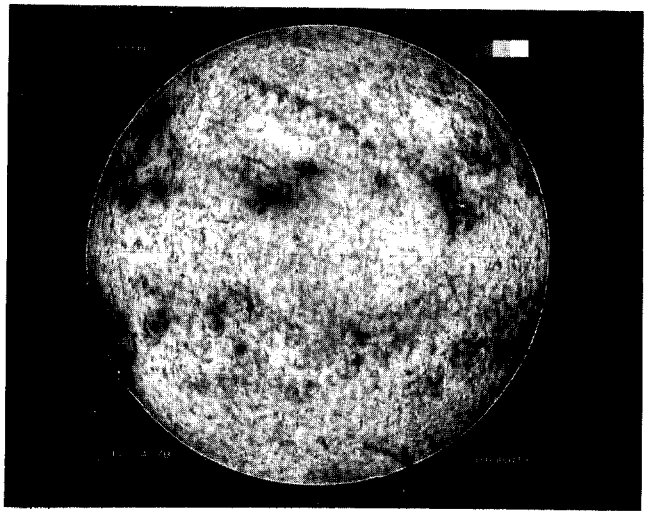

Figure 1-18. A sample 10830 Å scan obtained by the National Solar Observatory at Kitt Peak on 24 Dec 1978. Active Regions and prominences are black and coronal holes are light. Defining a coronal hole usually requires a series of pictures taken over several days as well as information about the magnetic field.

it is probably through the emergence, growth, transport and destruction of magnetic flux that the sun produces the transient behavior which causes large responses in the earth's environment.

1.2.1 The Sunspot Cycle

The most obvious manifestation of solar activity is the 11-year sunspot cycle. The *relative sunspot number R* (or Wolf or Zurich number) remains the single most important index for the general level of solar activity; it is calculated according to the formula

$$R = k(n + 10g),$$

where n is the number of individual spots visible on the solar disk, g is the number of sunspot groups (see below), and k is a station constant, or "personal equation" for the particular observatory.

Records of sunspot counts have been kept since the mid-seventeenth century (Figure 1-19). The cyclic behavior of R with a period averaging 11.4 years is the most obvious feature in the historical record, although an approximately 80-year periodicity may also be present. The anomalous period of low activity, 1645-1700 (*Maunder mimimum*), is recognized as a possible reduction in the level of solar activity; its existence has been independently supported by measurements of the carbon-14 content in tree rings formed during that era.

Most sunspots occur in groups that are dominated by a leader spot on the western side of the group and one or more trailer spots to the east (Figure 1-20); the leader spot is often the largest spot within the group. Magnetic fields in large spots are typically 3000 gauss, with leader and trailer spots generally having opposite polarities. During an 11-year cycle all leader spots in the northern hemisphere of the sun have one magnetic polarity, while in the southern hemisphere this polarity is reversed. This pattern persists throughout the rise and decline of the cycle. During the next cycle, however, the entire polarity pattern is reversed. Thus, the fundamental cycle of solar magnetic activity is actually about 23 years in duration. During cycle No. 21 (maximum in 1979-80), leader spots in the northern hemisphere had positive polarity (magnetic vector pointing outward from the solar surface).

The first sunspots of a new cycle typically appear at latitudes of 20° to 25° in both northern and southern hemispheres. As the cycle progresses, additional spots appear at lower latitudes, until they are concentrated near the equator at the end of the cycle (Figure 1-21).

Major variations in coronal structure take place during the solar cycle. Several decades of observations have confirmed that green-line intensities, and to some extent the red-line intensities, follow the sunspot number quite well. In particular, averages of the green-line intensities show large maxima at midlatitudes in both hemispheres that appear near or coincident with sunspot latitudes. These belts move towards the equator with the progression of the solar cycle and finally merge.

The total variation of the green-line intensity during a solar cycle is significant. In addition, the appearance of the two yellow lines is now known to be an excellent indicator of regions which will produce large flares and perhaps even proton events.

1.2.2 The Solar Dipole Magnetic Field

The sun has a weak dipole magnetic field aligned with its axis of rotation. Because of the stronger, complex field patterns associated with spot groups, however, this dipole field is recognizable only at latitudes above 60°, where it measures about 1 gauss on the solar surface. It is believed that the dipole field, although weak in general, becomes concentrated in the midlatitudes due to the dynamo action of the sun's differential rotation. *Magnetic ropes* of strong field may then rise to the surface due to magnetic buoyancy, forming the oppositely-poled leader and trailer portions of an active region where the flux loop intersects the photosphere. This would account for the spot-polarity law discussed above. The loops may eventually rise into the outer corona where they neutralize the original dipole field and ultimately replace it with a new dipole field of opposite sign. The polarity reversal of the dipole field occurs near sunspot maximum although the spot polarities themselves remain consistent with the polarity of the dipole field that existed at the beginning of the cycle.

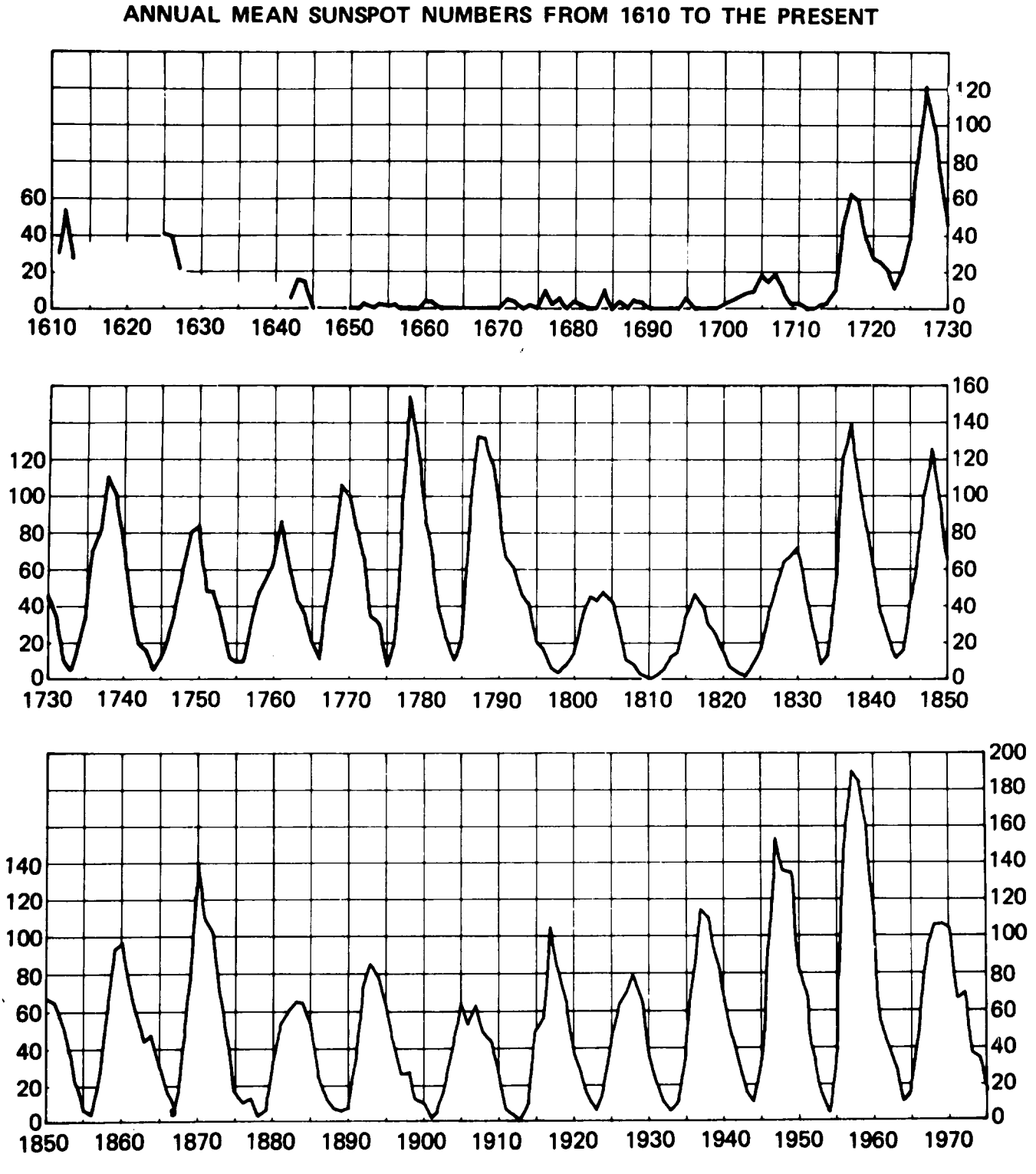

Figure 1-19. Annual mean sunspot numbers from 1610 to 1975 (From Waldmeier [1961] and Eddy [1976] et al.)

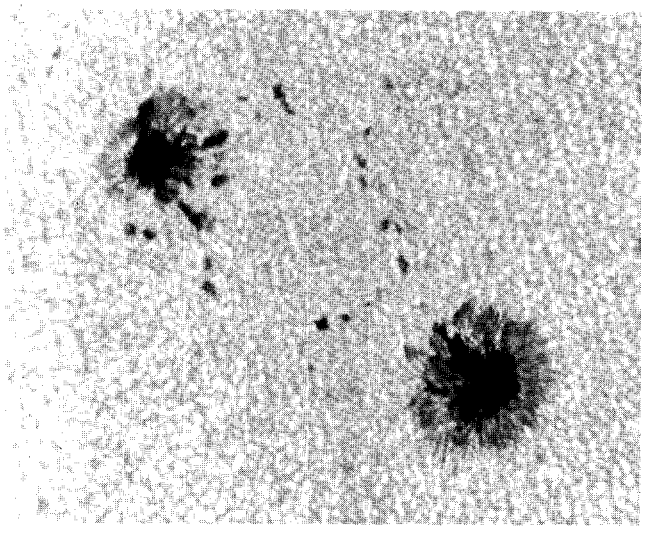

Figure 1-20. Typical bipolar sunspot group showing leader spot (right) and trailer spot. The background pattern of granulation is also visible (National Solar Observatory at Sacramento Peak).

1.2.3 The Emergence and Organization of Magnetic Flux

The solar surface abounds with both large and small-scale magnetic features. The smallest features, known as *filigree* (Figure 1-22) are bright, wiggly structures with lengths of 1 to 5 Mm and narrow widths of 100 to 200 km. They may, in fact, be smaller, but it has been impossible to date to see smaller structures with solar telescopes. Filigree reside in intergranular lanes and are visible with ground-based telescopes only on rare occasions when the atmospheric seeing allows the 1/4 arcsec resolution required to see them. Their locations are presumed to coincide with extremely fine magnetic structures occupying the granule boundaries, perhaps analogous to the somewhat larger flux tubes of the supergranule network (Section 1.1.3.2). Measurements show that these small flux tubes have intense magnetic fields with strengths between 1000 and 2000 gauss.

1.2.3.1 Active Regions. The development of a large-scale sunspot-bearing *active region* usually begins with an increase in the number and intensity of magnetic flux tubes in the photospheric network. In response to this, a brightening in the overlying chromosphere develops. These brightenings, or *plages* are the chromospheric counterparts to the sunspot group that later becomes visible in the photospheric layers. The corona responds also, producing a large area of bright emission visible, for example, in x-ray and radio images (Figure 1-23). Within a day of plage formation a small leader spot emerges which continues to grow in size for several days. The trailer spots usually form within a day of the leader, and many smaller spots often form throughout the entire region (Figure 1-20). Generally a sunspot begins life as a small *pore* which darkens as a con-

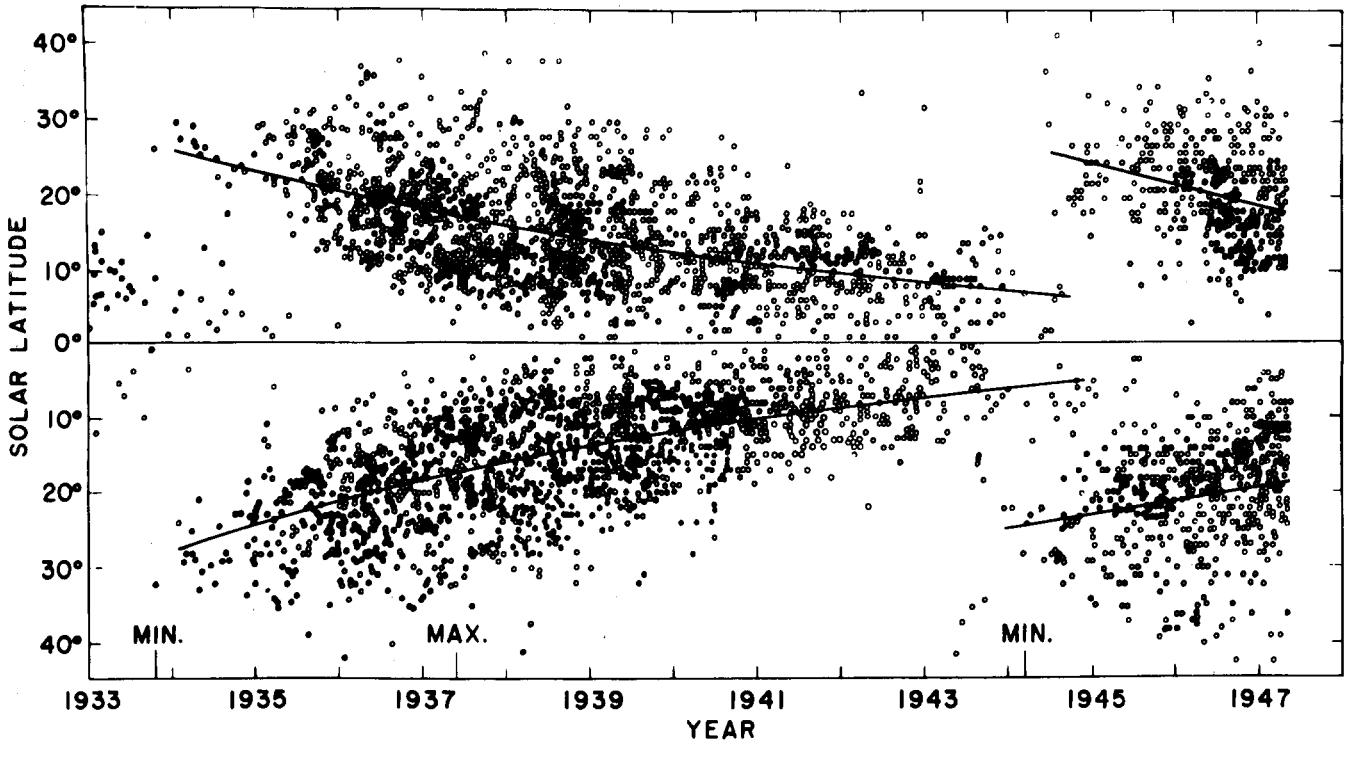

Figure 1-21. Typical "butterfly" diagram showing variation in distribution of sunspots with time. During a sunspot cycle the distribution migrates toward the solar equator (Mount Wilson and Las Campanas Observatories).

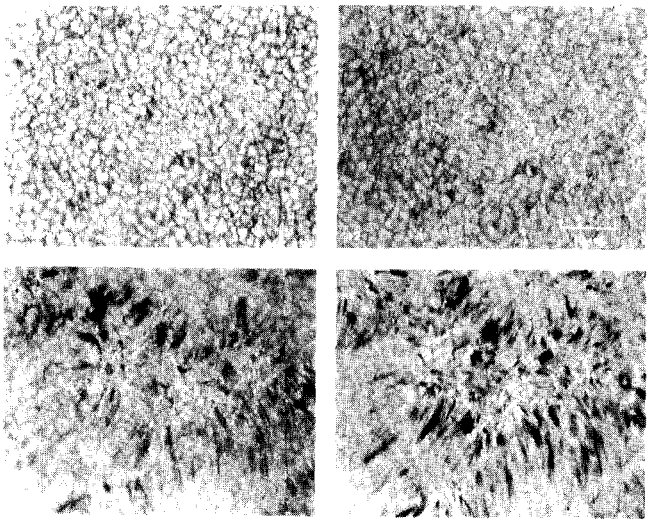

Figure 1-22. The solar filigree are visible as bright, wiggly structures lying in the intergranule zones. This series of filtergrams was taken in different wavelengths (clockwise from upper left): continuum, Hα + 2 Å Hα + 7/8 Å, Hα − 7/8 Å (National Solar Observatory at Sacramento Peak).

sequence of temperature reduction. The temperature drop is probably caused by the presence of the magnetic field, which may inhibit the supply of convective energy to the photosphere at that location, and/or may enhance the photospheric dissipation of energy at that point. The largest spots attain areas of 3×10^9 km^2 and temperatures 2000 K lower than the surrounding photosphere.

Sunspot groups usually reach maturity within several days after which they begin a slow decline. The leader spot

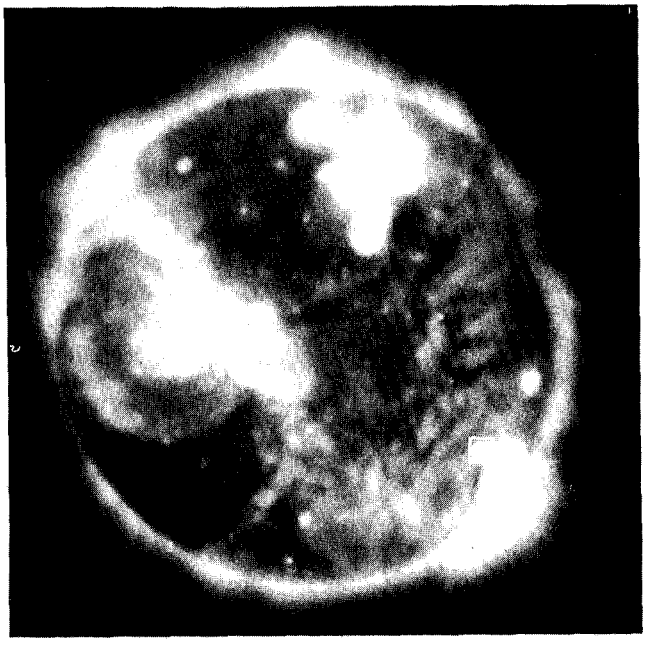

Figure 1-23. Soft x-ray photograph of the sun, showing the bright loop structures of active regions (John Davis, American Science and Engineering, Inc.).

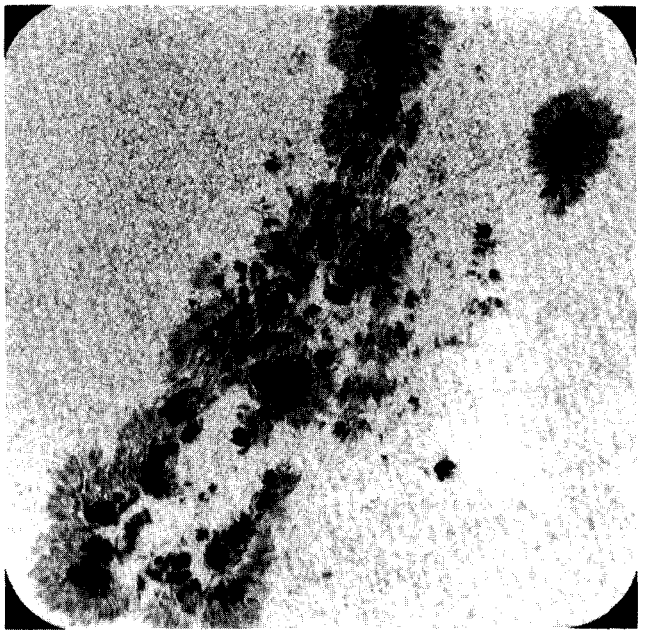

Figure 1-24. Complex sunspot group (National Solar Observatory at Sacramento Peak).

is the last to dissolve and occasionally may last for several months. The chromospheric plage persists even after all spots have disappeared.

A small number of active regions violate the simple polarity rule, and instead form complex magnetic structures with reversed or mixed polarities (Figure 1-24). These groups are responsible for nearly all the highly active solar phenomena (Section 1.2.6).

1.2.3.2 Ephemeral Regions. A significant portion of the total magnetic flux on the solar surface resides in *ephemeral active regions*. These are miniature bipolar regions of size ~ 30 Mm with average lifetimes of 12 hours. Although not usually associated with sunspots of their own, they are, nevertheless, legitimate active regions in the sense that they affect the chromospheric structures and develop visible plages. There may be several hundred such regions on the sun at any given moment, although like spots their numbers vary with the 11-year cycle. Their magnetic orientation, however, appears to be far more random than the leader and trailer polarities of sunspot groups.

1.2.4 Prominences

Prominences are large clouds of gas high above the chromosphere, visible as bright flame-like objects with emission spectra against the sky background at the limb, or as long rope-like *dark filaments* with absorption spectra against the solar disk. *Quiescent prominences* (Figure 1-25) are not associated with active regions, but rather form boundaries between very large-scale weak magnetic features

Figure 1-25. Quiescent prominence seen on the solar limb (National Solar Observatory at Sacramento Peak).

Figure 1-26a. Surge prominence associated with a flare seen near the solar limb (National Solar Observatory at Sacramento Peak).

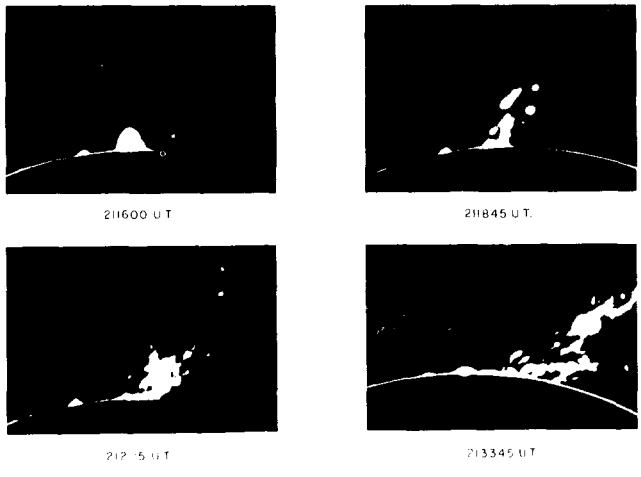

Figure 1-26b. Sequence showing development of a spray prominence associated with a flare (National Solar Observatory at Sacramento Peak).

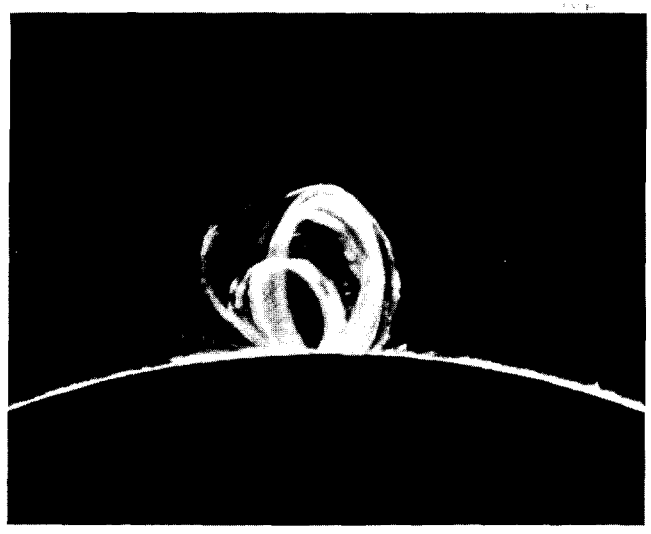

Figure 1-26c. Post-flare loop prominence (National Solar Observatory at Sacramento Peak).

in the quiet sun. They are the largest visible structures on the sun, sometimes reaching lengths exceeding a solar radius. Occasionally, quiescent prominences suddenly become active, erupt and blow off to great heights in the corona.

Other types of prominence-related phenomena include *surges, sprays,* and *loops* (Figure 1-26). These structures are often associated with flares as discussed below. They are, nevertheless, similar to quiescent prominences in the sense that their temperatures (10 000 K to 20 000 K) remain chromospheric even though their structures extend to coronal heights where the ambient temperatures are 100 times higher than their own.

1.2.5 Coronal Magnetic Fields

Careful observations also show a great spatial variation in the nature, if not the magnitude, of the magnetic field that threads its way through the corona. Bright regions tend to correlate with *closed-field regions* where models or observations indicate that the magnetic lines of force emerge from and re-enter the photosphere over scales less than a solar radius (Figure 1-23). Conversely, dark regions correlate with *open-field regions,* mysterious magnetic monopoles whose field lines may re-enter the sun again only after some convoluted journey through interplanetary space.

1.2.6 Flares

A *flare* is a transient, localized release of energy usually occurring in and above an active region. Flares produce greatly enhanced emissions spanning the entire electromagnetic spectrum and may accelerate particles to energies as high as 50 GeV. The flare eruption affects the corona, chro-

mosphere, and probably even the upper photosphere. The energy released by a flare ranges from 10^{29} to 10^{32} erg; durations vary from 1 to 100 minutes.

Flare *importance* has traditionally been assigned according to the flare's maximum area as observed in the Hα line (Table 1-4). Following the importance class, a letter code (F, N or B) is given to designate the relative brightness of the flare as faint, normal, or bright. In recent years flare importance has been supplemented by the soft x ray classification of the flare (Table 1-5). These x ray classes are only roughly correlated with the optical importances.

Table 1-4. Flare optical importance

Importance	Area (Heliographic Square Degrees)
S (Subflare)	2.06
1	2.06 to 5.15
2	5.15 to 12.4
3	12.4 to 24.7
4	>24.7

Table 1-5. Flare x ray classification

Class	1-8Å x ray flux at 1AU (W/m^2)
C	$10^{-6} \leq E < 10^{-5}$
M	$10^{-5} \leq E < 10^{-4}$
X	$E \geq 10^{-4}$

Historically, flares have been studied in the Hα line, which is formed in the chromosphere. Observations in the EUV and x ray regions, however, have shown that flares may be more correctly characterized as coronal phenomena with the primary energy release probably occurring in the low corona or transition region. It is not surprising, therefore, that flares are best seen in wavelengths originating in the corona. Flare images in soft x rays (1-10 Å) and XUV lines (200-300 Å) obtained by the Skylab Mission show that the basic flare structure is a low-lying coronal loop on the order of 20-50 Mm in length (Figure 1-27), wherein temperatures rise from the normal 1×10^6 K to about 20×10^6 K. Complex flares often reveal the presence of many such loop structures. The loop structures are formed by magnetic fields rooted in the deeper photospheric layers. The chromospheric flare (Figure 1-28), which is probably a secondary response to the coronal energy source, is primarily confined to the footprints of these loops forming intense flare *kernels*, or an arcade of loops may be involved forming a pair of serpentine, parallel *ribbons*. Magnetograph observations reveal opposite magnetic polarities for the two members of a kernel or ribbon pair. Photospheric field strengths for the flare loop footprints are typically 1000-2000 gauss

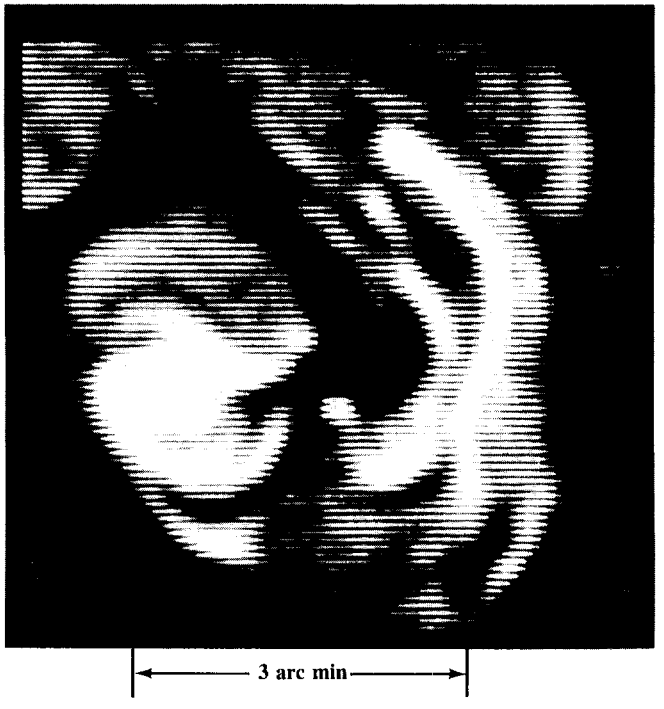

Figure 1-27. Soft x-ray loop structures in a flare (American Science and Engineering, Inc.).

Figure 1-28. Hα filtergram showing the chromospheric component of a "two-ribbon" flare (National Solar Observatory at Sacramento Peak).

for highly energetic events. Only rarely does the flare disturbance affect layers deep enough in the atmosphere to produce optical continuum (so-called *white-light flares*).

About half of all flares show a sudden or explosive rise to maximum. This *impulsive phase* is most clearly defined by hard x rays (photon energies 10 KeV - 1 MeV) or microwaves (wavelengths 1-30 cm) and may last only a minute in the case of simple flares. Soft x ray and Hα emissions, even in impulsive flares, are usually less abrupt in their onset, and often continue to rise after the impulsive components are in decline. Complex flares show multiple impulsive phases, with each impulse apparently being associated with a particular point in the flare. The impulsive components probably originate in a process which accelerates electrons to energies exceeding 10 KeV, producing hard x rays via electron-proton bremsstrahlung and microwaves via gyrosynchrotron radiation in the ambient magnetic fields (Chapter 11). Type III meter-wave radio bursts (Chapter 11), which may also occur during the impulsive phase, have been attributed to the outward escape of some of these electrons along open field lines. Recently obtained hard x ray images show the early stages of the hard x ray bursts occurring at loop footprints similar to the first optical kernel brightenings. This suggests a common energizing source in the loop, from which electrons are guided downward into the chromosphere along the field lines. It is not clear whether the population of electrons producing the impulsive emissions is best characterized as thermal or non-thermal. Certainly the hard x ray kernels and Type III radio bursts suggest a non-thermal directivity in the particles. If the energy distribution is thermal, then temperatures exceeding 10^8 K, and possibly even 10^9 K, would be required in order to produce the observed hard x ray continuum. The presence of protons with energies exceeding 30 MeV, as evidenced by nuclear gamma-ray lines in the impulsive phases of large flares, lends additional support to acceleration processes which produce non-thermal distributions.

A variety of phenomena occur in response to violent heating or magnetic rearrangement associated with flares. *Surges* (Figure 1-26) are spikes or filaments of chromospheric material sent outward (velocity ~ 100 km/s) by a sudden change in the distribution of magnetic field lines in the active region. Surprisingly, many surges are not associated with flares, although conversely a large fraction of flares seem to generate surges. The material pushed upward in a surge usually descends along its original trajectory. The latter characteristic distinguishes surges from *sprays* (Figure 1-26) which are high velocity (exceeding the solar escape velocity, 670 km/s) explosive ejections associated with certain flares.

The intense heating in flares usually "evaporates" the chromosphere near the bases of magnetic loops. The heated gas then rises to fill the loop with soft x ray-emitting plasma. Optically, these *post-flare loops* or *loop prominences* are often observed to form in the late stages of large two-ribbon flares (Figures 1-26). The enhanced soft x ray and ultraviolet flare emissions are responsible for a variety of immediate geophysical effects collectively known as *sudden ionospheric disturbances* (SIDs) (Chapter 10). These disturbances are a result of increased ionization at several levels in the ionosphere.

Shock waves produced by explosive heating propagate upward through the corona where they accelerate electrons and protons to relativistic energies. The interaction of shocks, particles, and magnetic fields generates Type II and Type IV meter-wave radio bursts (Chapter 11). The outward-propagating shock (velocity ~ 1000 km/s) is apparently also the origin of solar protons (energies ≥10 MeV) that produce terrestrial *polar cap absorption* (PCA) and solar cosmic ray *ground-level events* (GLE), while the shock wave itself arriving at the earth in about two days is a cause of the sudden commencement phase of geomagnetic storms (Chapter 4).

The origin of flares, particularly the processes of energy storage and release as well as the triggering instability, remains a difficult theoretical problem. Obviously, the local magnetic field is involved. Recent theories point to current-carrying magnetic configurations in which field lines reconnect and simplify. The problem is observationally difficult because the flare plasma parameters cannot be tracked in sufficient spatial and temporal detail. Without the aid of *in situ* measurements we are forced to rely upon observations of secondary effects which detect the flare energy only after disordering processes have already occurred.

1.2.7 Coronal Activity

1.2.7.1. Coronal Holes and Solar Wind. During Skylab, pictures of the sun were taken regularly with a soft x-ray telescope [Timothy et al., 1975], while at the same time 27-day recurrent geomagnetic disturbances were occurring. It was noticed that when areas dark in x rays crossed the central meridian near the sub-earth point, a geomagnetic disturbance occurred a few days later. This relationship persisted, and thus the source of the disturbances, the long-puzzling solar *M-regions,* was finally discovered, solving a riddle that had existed for decades. These dark areas named coronal holes (Figure 1-29) were shown to be sources of high-speed solar wind streams (HSS) that eventually impacted on the magnetosphere and caused the disturbances. For more information on HSS see Chapter 3.

Subsequent work on the nature of coronal holes has shown that they are somewhat cooler (by 500 000 K) than surrounding areas and up to an order of magnitude less dense. See Table 1-3. They also coincide with large areas of open magnetic field. It is thus hypothesized that an open field provides an unrestricted path for the propagation of solar wind into interplanetary space resulting in high solar wind speeds that deplete the matter in the holes and carry away internal energy (thus the lower density and temperature).

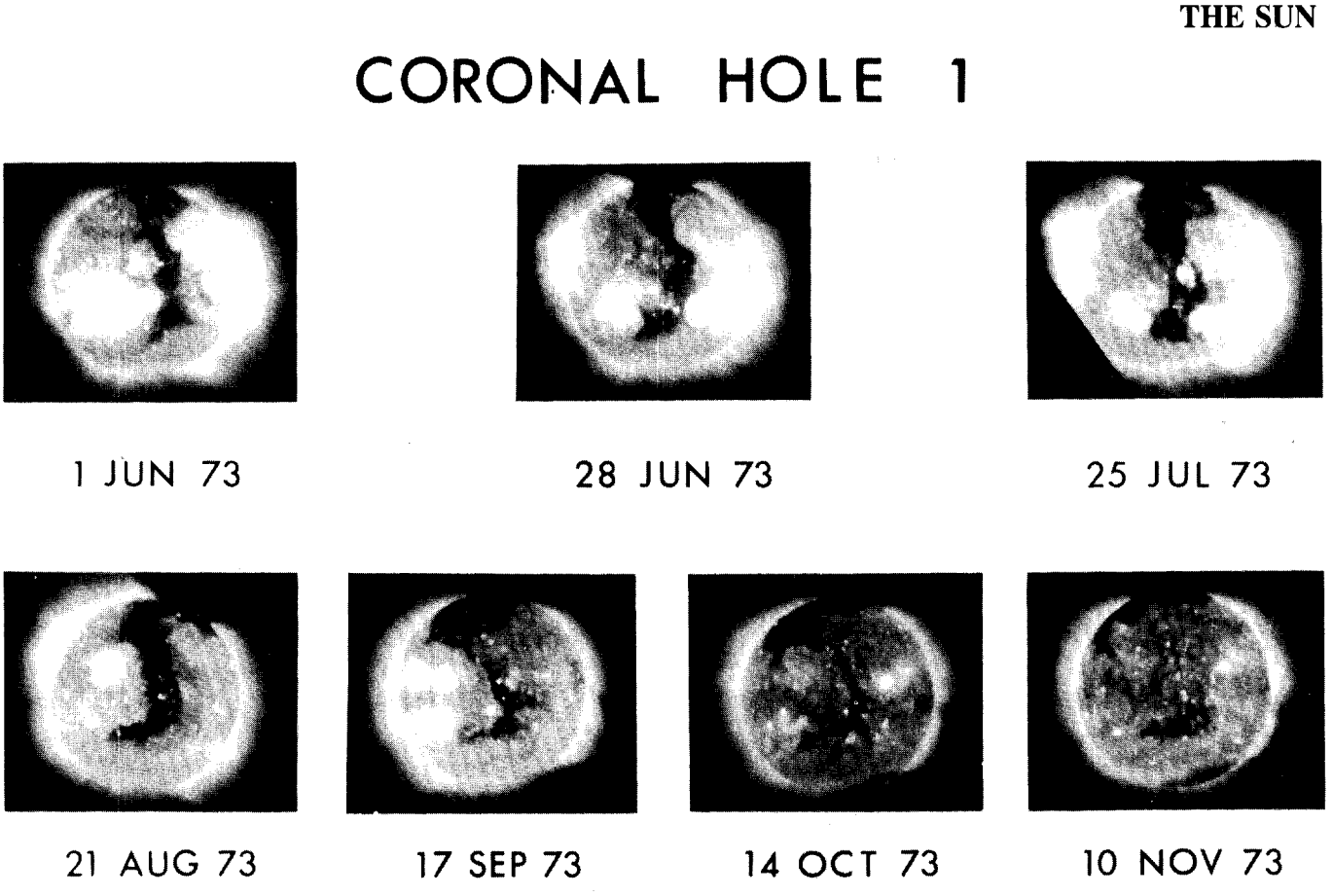

Figure 1-29. The first coronal hole ever observed in extensive detail. This series of pictures from Skylab shows the long-lived nature of the black coronal hole in the center of the disk as seen over several solar rotations (American Science and Engineering, Inc.).

1.2.7.2 Streamers. Earlier speculation on the source of M-regions had centered on *streamers,* which are long, radially-oriented bright regions of the corona. Recent research has shown that streamers can be detected even at the orbit of the earth. The signature of streamers [Borrini et al., 1981] consists of low solar wind velocity (on the order of 350 km/s), an increase in density and a decrease in the He/H ratio. These events appear to be coincident with *sector boundary* passages, which are sudden reversals of the interplanetary magnetic field (IMF) that often separate HSS from one another (Section 1.2.7.3).

1.2.7.3. The Solar Current Sheet. In the upper corona, magnetic fields tend to be mostly radially oriented and to reflect the polarity of the large-scale average field underlying them. Opposing fields in such large quasi-unipolar regions tend to reconnect at low altitudes, resulting in a single polarity remaining at high altitude drawn out from the sun by the solar wind. As the fields are stretched, they remain attached to the rotating sun "beneath" them, and each field line becomes a spiral (Chapter 3, Figure 2).

Although the sun tends to have a dominant polarity in each hemisphere, polarities from one hemisphere often intrude partially into the other. Thus as the sun rotates and this complicated pattern of fields is drawn out into space, a very complex neutral sheet or current sheet separating the two polarities develops (Figure 1-30).

As this pattern sweeps by the earth (or any other point near the ecliptic), it results in several days of one IMF polarity, followed by a sudden reversal and several days of

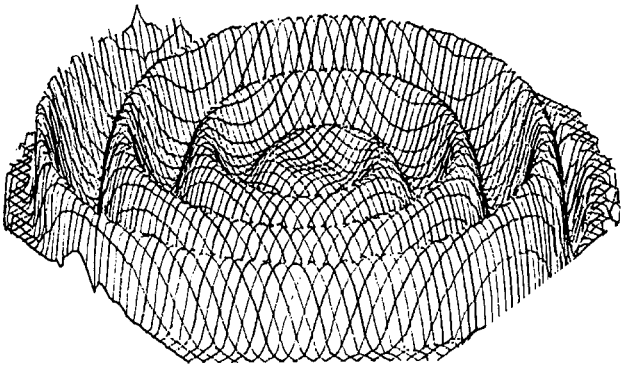

Figure 1-30. Schematic illustation of the warped solar current sheet. This undulating surface divides regions in interplanetary space having magnetic field pointing away from or toward the sun. The region covered by this diagram is approximately 20 astronomical units [Hakamada and Akasofu, 1982].

the opposite polarity. This yields a regular pattern of *magnetic sectors* separated by sector boundaries, which as we saw above are the signatures of coronal streamers sweeping by the earth. Distortions of the IMF also occur as the flare streams overtake slower streams and shocks are generated (Chapter 3). For further information refer to Hakamada and Akasofu [1982].

1.2.7.4 Transients. Skylab observations demonstrated the existence of a phenomenon never before observed outside of radio frequencies in the upper corona: the *coronal transient*. Fast motions had been observed in the lower corona, but the limited height range observable with ground-based coronagraphs gave no indication of their enormous size. Skylab showed huge bubble-shaped disturbances rising through the corona and expanding until their size approached that of the sun itself (Figure 1-31). As they enter the interplanetary medium, the transients may generate a shock wave that sweeps out into space. Their origin has been traced to surges or prominence eruptions.

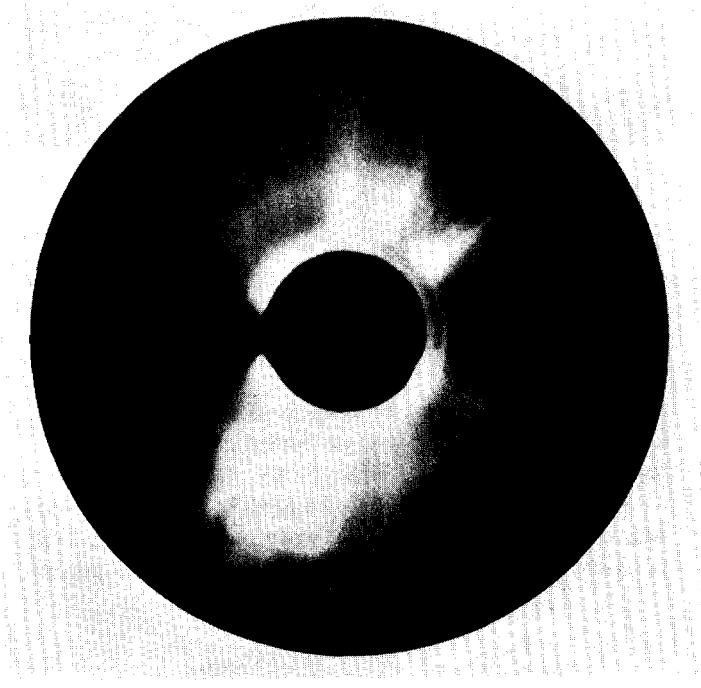

Figure 1-31. White-light photograph of a coronal transient obtained with the High Altitude Observatory white-light coronograph experiment on Skylab. The black circle is not the sun but the occulting disc of the instrument used to block out photospheric light. The size of its image is two solar radii. This particular transient traveled outward from the sun at about 500 km/s.

1.2.7.5 Coronal Induced Disturbances. Direct effects of the corona on communications and electronic systems on and near the earth come mainly through the very short-lived electromagnetic and particle emissions connected with solar flares. However, minor effects may occur due to the variation of radiation from the very highly-ionized elements of the corona. As solar active regions and their associated streamers grow and decay, rotate across the disk, and change in number with the solar cycle, the amount of high-energy radiation falling on the ionosphere varies slowly. Parameters such as the Maximum Usable Frequency (MUF) for long-range communications are partially controlled by the structure of the corona, and knowledge of this structure aids in the prediction of such parameters.

Indirect effects of the corona are manifested through propagation of coronal parameters to the earth by means of the solar wind (Chapter 3). Since solar wind conditions are directly controlled by the corona, the velocity, density, and magnetic field direction and magnitude of the solar wind are all determined at or near the solar surface. It is these parameters that determine whether a geomagnetic disturbance will occur. Geomagnetic disturbances generally indicate the onset of a wide variety of particle and electromagnetic-radiation effects in the geosphere, which together or separately have wide-ranging effects on a number of systems. In addition, Altrock [1980] has found that even if conditions in the solar wind are not conducive to the onset of a geomagnetic disturbance, changes in upper-atmospheric density may occur that affect satellite orbits. The change may be connected with the passage of streamers at the earth. Thus, in order to predict and/or protect against such detrimental effects, it is essential to have a thorough observational and theoretical understanding of processes in the solar corona.

1.2.8 Solar Variability and Climate

While the spectacular and explosive events associated with solar flares have immediate consequences upon the geophysical environment, the radiant energy output of the sun is a fundamental factor controlling the earth's climate. Although we do not yet have a firm, quantitative measure of the sensitivity of the earth's climate and weather to changes in the solar irradiance, climatologists estimate that the earth's mean surface temperature would change by about 1 K in response to a sustained 1% change in the total solar irradiance. The effects of a small change in the mean temperature could be large. An increase of two or three degrees, for example, would suffice to melt the polar icecaps, raise the sea level by several hundred feet and flood large areas of present coastland. On the other hand, a one degree decrease would have a significant adverse impact on the major grain producing regions of Europe and North America, and a decrease of perhaps ten degrees would probably result in total glaciation of the earth.

Fortunately, the total solar irradiance appears to be relatively constant, although this fact has proven rather difficult to verify. Ground-based irradiance measurements require

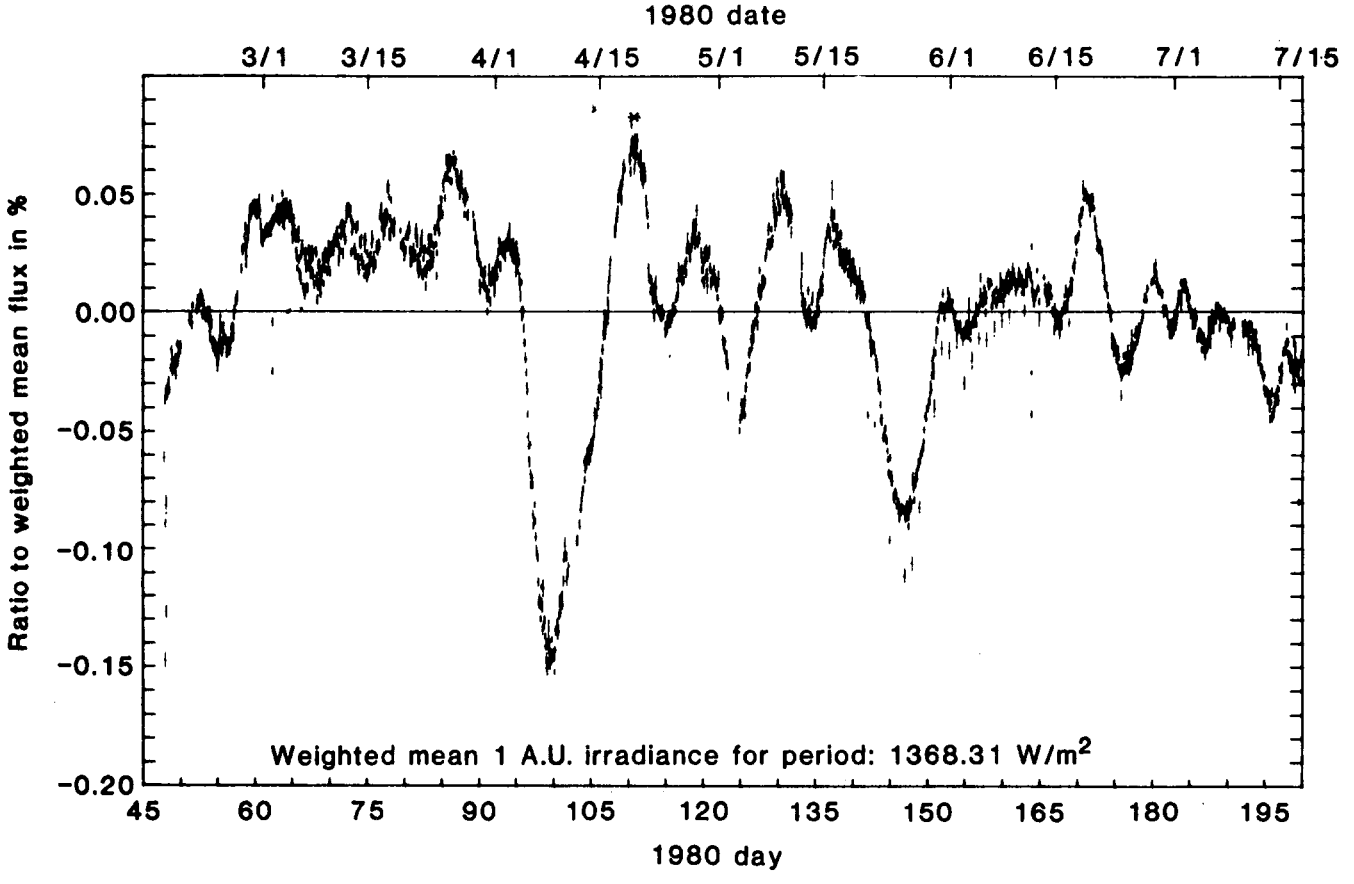

Figure 1-32. Total solar irradiance at 1 AU, shown as a percentage variation about the weighted mean for the first 153 days of SMM.

large corrections for atmospheric absorption, which is both highly selective and variable. Consequently, such measurements cannot achieve an accuracy better than ± 0.2%. Measurements from spacecraft have until only recently been limited to a comparable accuracy due to detector drift problems caused by exposure to the harsh space environment.

The variability of the solar irradiance in the ultraviolet and radio portions of the spectrum is well-established (Chapters 2 and 11) and is clearly associated with various manifestations of solar magnetic activity such as flares. Furthermore, the SMM radiometer measurements have clearly detected short-term fluctuations of 0.1-0.2% in the total irradiance (Figure 1-32) that correlate with the passage of large sunspot groups across the face of the sun. However, longer term trends have been more difficult to establish. Because there is no long term information from space-borne instruments, ground-based measurements still provide the best information concerning such trends. There is some marginal evidence, based on measurements of light reflected from solar system bodies as well as direct radiometry, for a slight increase of about 0.4% in total irradiance between 1968 and 1978. On the other hand, other ground-based radiometric measurements show no evidence for any variation exceeding 0.2% over the 30 year interval from 1923 to 1952. For more information refer to White [1977].

1.2.9 Predictions of Geophysical Disturbances

1.2.9.1 Flare Prediction. Flare-induced geophysical disturbances adversely affect many communications, navigation, and other electronic systems. Therefore daily predictions for the level of flare activity are issued by the joint USAF/NOAA (National Oceanic and Atmospheric Administration) Space Environment Services Center (SESC) located in Boulder, Colorado, working with Air Force Global Weather Central (GWC), Offutt Air Force Base, Nebraska. Present techniques for preparing solar forecasts are based on empirical relationships between flare occurrence and other active region parameters such as sunspot group type, magnetic complexity, and region evolution characteristics.

Most of the data used at SESC is provided by the Solar Electro-Optical Network (SEON) operated by the USAF Air Weather Service. SEON consists both of optical telescopes (SOON - Solar Observing Optical Network) and radio telescopes (RSTN - Radio Solar Telescope Network). The selection of the final SEON site (southeastern Italy) was announced in September 1982. SOON sites are located at five (four sites already operational in 1980) widely-spaced longitudes, providing continuous 24-hour monitoring capability. SOON provides data on solar magnetic configu-

rations, sunspot types and locations, and chromospheric characteristics. Four SEON sites compose RSTN, which monitors solar background radio emission (10-cm flux) as well as the types and sizes of flare-associated radio bursts. SEON issues immediate reports of flare occurrences, importance, and locations for use at SESC and GWC.

The near-real time acquisition of solar data by SEON and other observatories, as well as present and planned satellite monitors, is making available daily a large number of parameters for each active region on the solar disk. This mass of data lends itself to computer programs using sophisticated statistical procedures to maximize the predictive capability of the data. One technique, using a variation of multivariate discriminant analysis (MVDA) developed at AFGL, has resulted in an objective flare forecast superior to the presently-used, subjectively-derived forecasts.

1.2.9.2 Coronal Disturbance Prediction. SESC also predicts geomagnetic disturbances due to coronal fluctuations as part of its daily program. Primary data sources come from the National Solar Observatory's Sacramento Peak coronal photometer and Kitt Peak HeI 10830 Å patrol, and the UCSD's radio scintillation program (Section 1.1.3.4).

REFERENCES

Allen, C.W., *Astrophysical Quantities,* Athlone Press, London, 1973.

Altrock, R.C., "Anomalous Satellite Drag and the Green-Line Corona," in *Solar-Terrestrial Predictions Proc.*, edited by R.F. Donnelly, NOAA, Boulder, **4:** E1-E4, 1980.

Athay, R. Grant (ed.), *The Solar Chromosphere and Corona: Quiet Sun, Astrophysics & Space Science Library,* **53**, D. Reidel, Dordrecht, Holland, 1976.

Billings, D.E., *A Guide to the Solar Corona,* Academic Press, New York, 1966.

Bonnet, R.M., "Contribution of OSO-8 to our Knowledge of the Chromosphere and Transition Region," *Space Sci. Rev.*, **29:** 131–200, 1981.

Borrini, G., J.T. Gosling, S.J. Bame, W.C. Feldman, and J.M. Wilcox, "Solar Wind Helium and Hydrogen Structure Near the Heliospheric Current Sheet: A Signal of Coronal Streamers at 1 AU," *J. Geophys. Res.*, **86:** 4565–4573, 1981.

Bray, R.J. and R.E. Loughhead, *Sunspots,* Wiley, New York, 1965.

Bray, R.J. and R.E. Loughhead, *The Solar Chromosphere,* Chapman & Hall, London, 1974.

Christensen-Dalsgaard, J. and D.O. Gough, "Towards a Heliological Inverse Problem," *Nature,* **259:** 89–95, 1976.

Donnelly, R.F. (ed.), *Solar Terrestrial Predictions Proceedings,* Vol. 1-4, U.S. Dept. of Comm., NOAA/ERL, Boulder, 1979–80.

Eddy, J.A. (ed.), *The New Solar Physics,* Westview Press, Boulder, 1978.

Eddy, J.A., P. A. Gilman, and D. E. Trotter, "Solar Rotation During the Maunder Minimum," *Sol. Phys.*, **46:**3–14, 1976.

Gibson, E.G., *The Quiet Sun,* NASA SP-303, NASA, U.S. GPO, Washington, D.C., 1973.

Gingerich, O., R.W. Noyes, and W. Kalkofen, "The Harvard-Smithsonian Reference Atmosphere," *Sol. Phys.*, **18:** 347–365, 1971.

Gough, D.O. (ed.), "Problems in Solar and Stellar Oscillations," Proc. 66th IAU Colloq., Crimean Astrophys. Obs., USSR, 1-5 Sep 1981, *Sol. Phys.*, **82**, 1983.

Hakamada, K. and S.-I. Akasofu, "Simulation of Three-Dimensional Solar Wind Disturbances and Resulting Geomagnetic Storms," *Space Sci. Rev.*, **31:** 3–70, 1982.

Hill, H.A., "Observational Evidence for Global Oscillations of the Sun: A Review," *Lecture Notes in Physics,* 125, Nonradial and Nonlinear Stellar Pulsation Workshop, Tucson, March 12–16, 1977, edited by H. Hill & W. Dziembowski, Springer-Verlag, New York, 1979.

Hill, H. A., R. T. Stebbins, and T. M. Brown, *Proceedings Fifth International Conference Atomic Masses and Fundamental Constants,* Gorden and Breach, New York, 1975.

Howard, R., and B.J. LaBonte, "The Sun is Observed to be a Torsional Oscillator with a Period of 11 Years," *Astrophys. J.*, **239:** L33–L36, 1980.

Jordan, S. (ed.), *The Sun as a Star,* NASA SP-450, 1981.

Kuiper, G.P., *The Sun,* University of Chicago Press, Chicago 1952.

November, L.J., J. Toomre, K.B. Gebbie, and G.W. Simon, "The Detection of Mesogranulation on the Sun," *Astrophys. J.*, **245:** L123–L126, 1981.

Rhodes, E.J., R.K. Ulrich, and G.W. Simon, "Observations of Non-Radial P-Mode Oscillations," *Astrophys. J.*, **218:** 910, 1977.

Sturrock, P. (ed.), *Solar Flares Skylab Workshop,* University of Colorado Press, Boulder, 1980.

Svestka, Z., *Solar Flares,* D. Reidel, Dordrecht, Holland, 1976.

Timothy, A.F., A.S. Krieger, and G.S. Viana, "The Structure and Evolution of Coronal Holes," *Sol. Phys.*, **42:** 135–156, 1975.

Vernazza, J.E., E.H. Avrett, and R. Loeser, "Structure of the Solar Chromosphere III. Models of the EUV Brightness Components of the Quiet Sun," *Astrophys. J. Suppl.*, **45:** 635–725, 1981.

Waldmeier, M. "The Sunspot Activity in the Years 1610–1960," Schulthess, Zurich, 1961.

White O.R. (ed.), *The Solar Output and its Variation,* Colorado Associated University Press, Boulder, 1977.

Wilcox, J.M. and R. Howard, "Differential Rotation of the Photospheric Magnetic Field," *Sol. Phys.*, **13:** 251–260, 1970.

Willson, R.C., S. Gulkis, M. Janssen, H.S. Hudson, and G.A. Chapman, "Observations of Solar Irradiance Variability," *Science,* **211:** 700–702, 1981.

Zirker, J.B. (ed.), *Coronal Holes and High Speed Wind Streams,* Colorado Associated University Press, Boulder, 1977.